Materials Advances

ROYAL SOCIETY OF CHEMISTRY

PAPER

View Article Online
View Journal

Cite this: DOI: 10.1039/d6ma00365f

Epoxy–glass fibre composite splash ring suppresses metal-derived lubricant contamination in splash lubrication systems

M. Essam El-Rafey,[a] Abbas E. Anwar,[a] Ahmed Abdelrahman,[b] Mervette El-Batouti [c] and Mahmoud M. Elewa *[d]

Received 23rd March 2026,
Accepted 22nd May 2026

DOI: 10.1039/d6ma00365f

rsc.li/materials-advances

Metallic components used in splash-lubricated mechanical systems can generate wear debris that accelerates lubricant degradation and contaminates the oil. In this work, a fibre-reinforced epoxy–glass composite splash ring was developed as a nonmetallic alternative to a conventional brass component. The composite ring was fabricated and evaluated in a laboratory lubrication rig operating at 3000 rpm for long-duration tests up to 1000 h. Oil samples were analysed using atomic absorption spectrometry, total acid number measurements, and gravimetric wear analysis, while surface morphology was examined by scanning electron microscopy. The composite component eliminated detectable Cu and Zn contamination in the lubricant and reduced oil oxidation, while increasing oil flow rate by approximately 66% compared with the brass reference component. The improved performance is attributed to the chemical inertness and favourable tribological behaviour of the epoxy–glass composite, which suppresses metal-catalysed oxidation reactions and reduces the generation of wear particles. These results demonstrate that fibre-reinforced polymer composites can provide an effective materials-based strategy for mitigating lubricant contamination and improving the operational reliability of splash-lubricated systems.

1. Introduction

1.1. The criticality of bearing lubrication in industrial machinery

Bearings are fundamental components in virtually all forms of rotating machinery, including industrial pumps, turbines, and compressors, where performance, reliability, and longevity are paramount.[1] Their primary function is to support rotating shafts, manage complex loads, and minimise friction between moving and stationary surfaces, thereby ensuring smooth and efficient operation.[2,3] Bearings are crucial to the reliability and service life of any mechanical system; if they fail, the whole system ceases to function. Nevertheless, due to the arduous conditions of contemporary industrial applications, which feature prolonged exposure to heavy loads and high speeds of rotation, rolling element bearings are particularly susceptible to malfunctioning and premature failure.[4] From research and industrial failure analysis, it appears that the main source of the majority of mechanical failures is improper or ineffective lubrication. Therefore, this becomes an area of paramount concern to ensure the safe, reliable, and continuous operation of critical equipment.[5] Improper lubrication is said to cause 36–50% of all machine failures, according to industry studies, which translates into a sizeable annual economic loss. Alone estimated at $240 billion. For a single large company, unplanned downtime can exceed $600 000 per h.

1.2. Limitations of conventional splash lubrication with metallic oil rings

Splash lubrication is a widely adopted, cost-effective method for delivering lubricant to bearings in low-to-moderate speed applications where the complexity and expense of a pressurised system are not justified.[6] In this arrangement, a loose-fitting oil ring hangs on the rotating shaft, dips into the oil sump, and splashes lubricant onto the bearings as the shaft rotates.[7] Despite its operational simplicity, the method harbours a critical design flaw when implemented with conventional metallic materials: brass and other copper–zinc alloy rings interact with the rotating shaft in an inherently unstable manner, generating unpredictable oscillation rather than smooth rotation.[8,9] These instabilities impose repeated impact and sliding contact at the ring–shaft interface, initiating mechanical wear and corrosion

[a] Materials Science Department, Institute of Graduate Studies and Research, Alexandria University, Alexandria, Egypt
[b] Western Desert Gas Complex, Egyptian Natural Gas Company - GASCO, Alexandria, Egypt
[c] Chemistry Department, Faculty of Science, Alexandria University, Alexandria, Egypt
[d] Arab Academy for Science, Technology and Maritime Transport, Alexandria, P. O 1029, Egypt. E-mail: mahmoud.elewa@aast.edu

of the ring itself.[10] Wear then triggers a destructive failure cascade, metallic debris enters the lubricant, where Cu^{2+} and Zn^{2+} ions act as catalysts for hydroperoxide decomposition, accelerating free-radical autoxidation, raising the total acid number (TAN), and reducing lubricity, which in turn accelerates further wear.[11] Contamination levels in field-aged oils from brass-ring systems routinely reach hundreds of ppm for both copper and zinc,[12,13] while the ring itself can lose up to 50% of its width in fewer than 10 000 h of service,[10] reducing oil delivery and compounding the degradation. These limitations collectively underscore the necessity for nonmetallic alternative materials capable of withstanding high-speed rotating conditions without contributing metallic debris to the lubricant.[14]

1.3. Material rationale for epoxy–glass composite splash rings

Polymer matrix composites (PMCs) offer a compelling alternative to conventional metallic splash rings by combining chemical inertness, low density, and corrosion immunity with competitive mechanical performance.[15–17] Among PMCs, epoxy–glass fibre systems are particularly well suited to this application: the thermosetting epoxy matrix provides dimensional stability, strong fibre–matrix adhesion, and resistance to lubricant-induced chemical attack, while E-glass reinforcement imparts the tensile stiffness and load-bearing capacity required to sustain dynamic shaft contact at 3000 rpm.[18–21] Critically, the nonmetallic composition eliminates the source of Cu, Zn, and Fe debris that initiates lubricant degradation in brass ring systems, breaking the failure cascade at its origin.[22,23] Detailed mechanical, thermal, and tribological property comparisons between the epoxy–glass composite and conventional brass are provided in Table S1.[24–26] Predictive frameworks for estimating erosion and wear in composite materials, including kinetic-energy-based models and Artificial Neural Network (ANN) approaches, are reviewed in the SI (Section S2) for readers seeking a theoretical basis for quantitative wear-rate estimation.[27]

1.4. Application and performance

• With friction reduced and sealing performance enhanced, the life of sealing rings is extended, and they can be made more effective in their application, like in high-speed rotating machines.[28,29]

• While electrical insulation was mentioned as one more benefit, adding an intermediate layer and protective coating would enhance erosion resistance.[30]

In increased erosion resistance, this should also involve trade-off considerations such as manufacturing complexity and cost. Besides, for the full realisation of the benefits, the context of these composites may have required adaptations to the design and maintenance of existing systems.

1.5. Study objectives

Despite extensive research on polymer composites for tribological applications, their use as a direct replacement for metallic oil splash rings, specifically to suppress lubricant metal-ion contamination and retard oxidative degradation, has not been systematically investigated.[19,31–34] This study addresses that gap by fabricating a short-fibre epoxy–glass composite ring (90 : 10 wt% epoxy : E-glass) and evaluating its performance against a conventional brass ring under controlled conditions (3000 rpm, ISO VG 68 mineral oil, up to 1000 h). The specific objectives are: (i) to quantify metallic wear-debris contamination (Cu, Zn, Fe by AAS) and lubricant oxidation (TAN by ASTM D664) as a function of ring material and test duration; (ii) to characterise composite ring wear and surface morphology by gravimetric analysis and SEM; and (iii) to assess lubrication efficiency (oil flow rate) and thermal loading (bearing housing temperature) to establish whether the composite ring maintains adequate functional performance across the test duration.

2. Materials and methods

A rigorous experimental and analytical methodology was established to fabricate and evaluate the new composite oil splash ring against the traditional materials. The protocol design was intended to simulate operational conditions and assess key performance indicators, including wear, lubrication, and structural durability.

2.1. Materials and composite ring fabrication

The test ring materials comprised: (A) a conventional brass ring (CuZn30, CW505L) as the primary metallic benchmark; (B) an HDPE ring as a polymeric control; and (C) the target composite ring (designation E1), consisting of 90 wt% Araldite LY 1564 epoxy resin cured with Aradur 3486 polyamide hardener and 10 wt% short-cut E-glass fibres. The E1 composite ring was fabricated by casting a homogeneous fibre–resin slurry into a custom mould dimensioned to match the standard metallic ring geometry (OD 80 mm, ID 50.1 mm, width 15 mm), followed by ambient-temperature cure.[35] Benchmark brass and HDPE rings were machined to identical dimensions by CNC turning.[36] All rings were verified to meet the dimensional and surface-finish specifications in Table 1A prior to testing. Full fabrication protocols, including resin-to-hardener ratio, fibre dispersion procedure, cure schedule, and preliminary material screening results (formulations D1–D3), are provided in Section S3.

2.2. Experimental apparatus

A test rig has been custom-made to test the performance of new polymeric-composite oil-splash rings under operating conditions. The test rig was designed to simulate high-speed rotating machinery conditions, with the following components: a shaft, bearings, and an oil reservoir. An induction motor drove the shaft *via* a belt-and-pulley system, with precise control of the rotational speed to.[37] The test rig geometry is fully specified in Fig. 1, with critical dimensions provided in millimetres. The oil splash ring (positioned 150 mm from the drive end) is immersed to a depth of 12 ± 0.5 mm in the oil sump, maintaining a working volume of 2.5 L of ISO VG 68 mineral oil. The shaft diameter is 35 mm, with radial bearings positioned at 100 mm and 250 mm from the drive end, respectively. The thrust bearing is located at the non-drive end. The oil level is maintained within ± 2 mm of the nominal

Table 1 Test rig operating parameters and conditions

Parameter	Value	Unit
Shaft speed	3000	rpm
Lubricant type	ISO VG 68 mineral oil	—
Oil sump temperature (initial)	25	°C
Radial load (calculated)	17	kN
Axial load (calculated)	45	kN
Test durations (screening/final)	500/1000	h
Ambient remperature	23 ± 2	°C

A. Dimensional and surface specifications of test rings

Parameter	Copper alloy ring	Epoxy–glass ring	HDPE ring
Outer diameter, D_o (mm)	80.00 ± 0.05	80.00 ± 0.05	80.00 ± 0.05
Inner diameter, D_i (mm)	50.10 ± 0.05	50.10 ± 0.05	50.10 ± 0.05
Ring width, *b*. (mm)	15.00 ± 0.05	15.00 ± 0.05	15.00 ± 0.05
Mass (g)	107.8 ± 0.1	12.2 ± 0.1	9.5 ± 0.1
Surface roughness, R_a (μm)	0.80 ± 0.05	0.85 ± 0.05	0.82 ± 0.05
Radial shaft clearance (mm)	0.05 ± 0.01	0.05 ± 0.01	0.05 ± 0.01
Axial end clearance to housing (mm)	0.50 ± 0.05	0.50 ± 0.05	0.50 ± 0.05

B. Composition of materials of bearing-oil splash ring, (% wt)

Material type	Polymer content (wt%)	Matrix material	Fibre content (wt%)	Fiber material	Ring weight (g)
Copper alloy, A	N.A.	N.A.	N.A.	N.A.	107.75
Carbon steel, B		N.A.	N.A.	N.A.	99.16
Polymeric, C	100% (HDPE)	N.A.	N.A.	N.A.	13.35
Composite, D1	90%	Unsaturated polyester	10%	Glass fibre	13.10
Composite, D2	85%	Unsaturated polyester	15%	Glass fibre	13.55
Composite, D3	80%	Unsaturated polyester	20%	Glass fibre	13.74
Composite, E1	90%	Epoxy	10%	Glass fibre	12.20

C.

Parameter	Unit/notes	Cu	Zn
Calibration range	mg L^{-1}	0.010–1.00	0.015–2.00
Calibration fit (R^2)	Linear regression	0.9992	0.9994
LOD	mg L^{-1} (3 × SDblank)	0.003	0.005
LOQ	mg L^{-1} (10 × SDblank)	0.010	0.015
Spike recovery (n = 5)	% mean ± SD	95.2 ± 4.1	97.8 ± 3.5
Repeatability	%RSD (n = 6)	3.8	3.1
Reproducibility	%RSD inter-day	~4.0	~5.9
Expanded uncertainty	% (k = 2)	~14	~15

12 mm immersion depth through periodic monitoring and top-up every 24 h.

The basic components of the rig are the following:

• A 2.2 kW variable speed induction motor that can run up to 3000 rpm with an impressive output capability.

• An industrial standard pump bearing housing modified to come with an integrated oil reservoir and housing radial and thrust bearings mounted within it.

• A steel shaft is mechanically coupled to the motor through a belt and pulley for precise speed control.

• Mounting features are provided on the shaft for the test oil splash ring, the lower edge of which is submerged in the oil sump.

The bearing configuration consists of:

– Two deep-groove ball bearings (SKF 6207-2Z) supporting radial loads, positioned in tandem at the drive end.

– One angular contact ball bearing (SKF 7207 BEP) at the non-drive end, accommodating combined radial and axial loads (45 kN axial capacity).

– Bearing clearances: radial clearance 0.015–0.035 mm (C3 fit), axial preload 0.08 mm *via* locknut adjustment.

Load distribution is achieved through a belt-and-pulley system with a 1 : 2.5 speed reduction ratio, delivering calculated radial loads of 17 kN and axial loads of 45 kN to the bearing assembly. Load verification was performed using strain gauges mounted on the shaft (calibration accuracy ±3%).

Operational parameters were monitored using sensors incorporated into the test rig during the experiments.

Ring dimensions (outer diameter, inner diameter, and width) were measured at three circumferential positions using a digital vernier calliper with 0.01 mm resolution and ±0.05 mm accuracy. Shaft–ring radial and axial clearances were checked by feeler gauges and confirmed on a coordinate measuring machine (CMM) for selected specimens. Surface roughness R_a of the running surfaces was measured using a contact stylus profilometer over a 4 mm evaluation length; three traces per ring were recorded and averaged. The values in Table 1A confirm that, within the stated tolerances, all rings share the same nominal geometry and

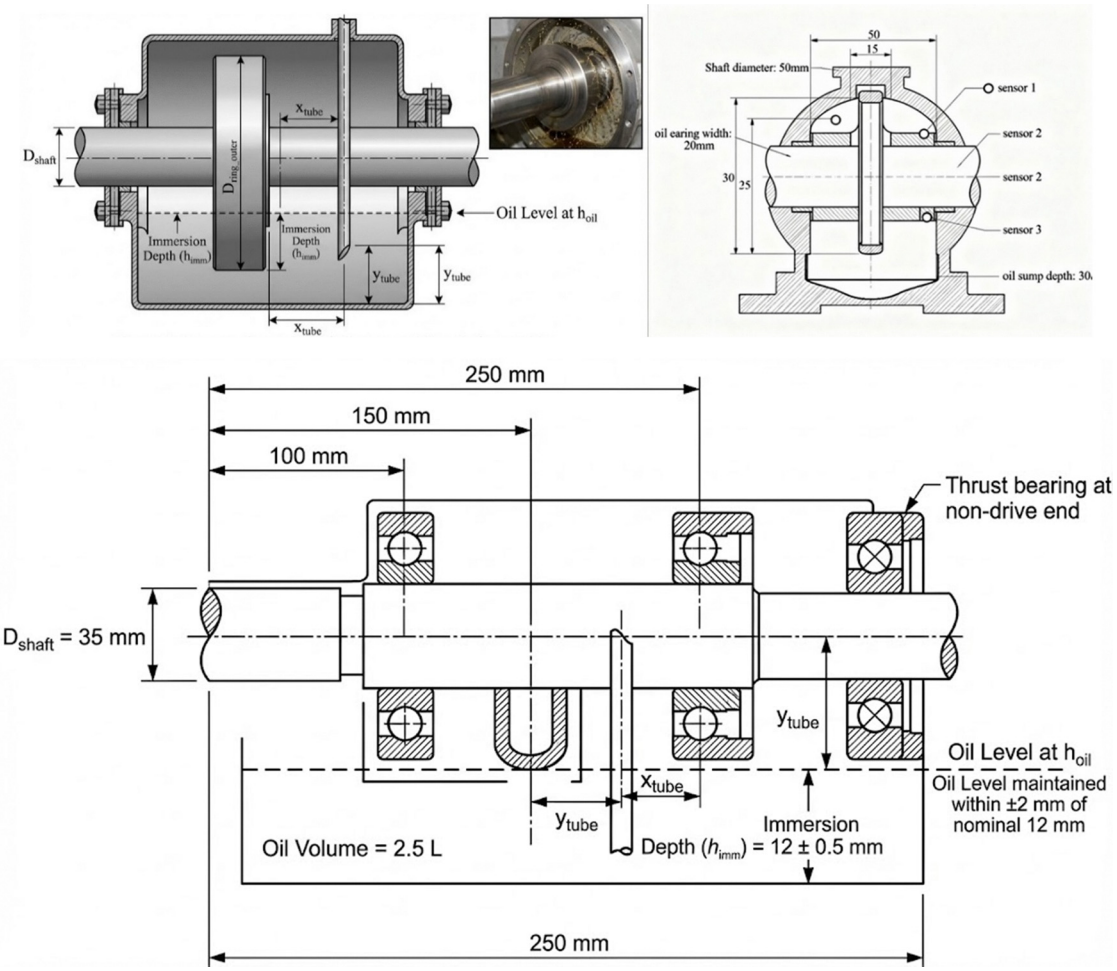

Fig. 1 Schematic of the oil splash ring test rig showing shaft, bearings, composite ring position and integrated oil sump for ISO VG 68 mineral oil at 3000 rpm.

clearances, so differences in performance can be attributed to material behaviour rather than geometric bias. Table 1B shows the Composition of materials of the oil splash ring.

2.2.1. Decontamination protocol between successive ring tests. To minimise cross-contamination of the lubricant between successive ring tests, a standardised solvent-cleaning and flushing protocol was applied after each run, including oil drainage, solvent washing of shaft and sump surfaces, ultrasonic cleaning of removable components, and replacement of seals and gaskets (full protocol: Section S4). The effectiveness of the procedure was verified by AAS analysis of the final rinse oil; residual Cu, Zn, and Fe concentrations after cleaning were consistently below 10 ppm for all elements, at least one order of magnitude lower than levels measured during copper-alloy ring tests, confirming that metallic carry-over between successive runs is negligible under the present experimental conditions.

2.2.2. Sampling strategy and experimental geometry. The test rig sump was filled with 2.50 ± 0.05 L of ISO VG 68 mineral oil, corresponding to a static oil depth of $H = 60 \pm 1$ measured from the sump floor. The oil splash ring, mounted on a 35 mm diameter shaft, had an outer diameter of 80 mm; at the nominal oil level, the lower edge of the ring was immersed by 12 ± 0.5, *i.e.*, approximately 15% of its diameter. This immersion depth was selected to ensure a stable splash regime while avoiding complete submergence of the ring.

Throughout each test, the oil level was checked every 24 h using a calibrated dipstick referenced to the housing datum, and the level was manually topped up with fresh oil whenever it deviated by more than 2 mm from the nominal 60 mm depth (mainly due to small evaporative losses). Under these conditions, the ring remained partially immersed (never less than 10 mm or more than 14 mm) over the entire 500–1000 h test period. A schematic of the sump, ring and oil level, including key dimensions and immersion depth, is provided in Fig. 1.

Oil samples were withdrawn from the sump at mid-depth and at a fixed horizontal location directly beneath the ring splash zone to obtain representative bulk oil while avoiding surface films and settled sludge. A stainless-steel sampling tube (internal diameter 4 mm, length 150 mm) was positioned so that its inlet was located 30 ± 2 below the instantaneous oil surface (*i.e.* at approximately half the oil depth) and 20 mm from the sump sidewall. This location was selected to minimise entrainment of air bubbles and to avoid dead zones at the bottom of the sump.

Oil sampling was carried out at the beginning of each test (0 h, fresh oil) and after 500 h for all rings, with an additional

sample after 1000 h for long-term tests. At each sampling time, three independent 50 mL aliquots were collected into pre-cleaned amber glass vials with PTFE-lined caps. Immediately after collection, the vials were labelled, stored at 4 ± 1 °C in the dark, and analysed within 7 days to minimise changes in TAN and dissolved metal content. Stability checks on stored control samples showed no statistically significant changes in TAN or Cu/Zn/Fe concentrations during this storage period, within the analytical uncertainty of the methods. Prior to TAN and AAS analysis, samples were allowed to equilibrate to room temperature (23 ± 2 °C).

2.3. Performance evaluation protocol

A comprehensive performance assessment was conducted using a variety of test protocols tailored to each ring.

• Wear and durability testing: each ring was subjected to long-term operation testing to assess durability. Initial assessments were conducted on all materials over 500 h, after which the most promising candidates were subjected to extended testing for 1000 h. Wear was determined gravimetrically by measuring the mass of the whole ring before and after testing using a high-precision digital analytical balance (accuracy: ±0.0001 g). This method was conducted in accordance with wear measurement standards such as ASTM G99. The percentage of weight loss was computed to measure the rate of corrosion and wear.[38]

The mass of each ring, before and after testing, was measured using an analytical balance with a readability of 0.1 mg and a repeatability of better than 0.2 mg. Each reported value represents the mean of three consecutive measurements, and the balance was calibrated daily using traceable Class E2 weights. This gravimetric procedure provides a detection limit for wear mass loss of about 0.3 mg, enabling quantitative comparison of subtle differences between materials.

• Thermal monitoring: thermal measurements were conducted using a handheld infrared laser thermometer (Model 62 MAX +, Fluke Corporation, stated accuracy ±1.0 °C over 0–100 °C and resolution 0.1 °C). Before the test series, the instrument was calibrated against a reference blackbody source set to 50 °C and cross-checked against a contact K-type thermocouple mounted on a steel block; agreement was within ±0.3 °C. The bearing housing surfaces were painted matte, and an emissivity of 0.95 was used for all measurements, as recommended for oxidised painted steel. All readings were taken at a fixed distance of 50 mm from the housing surface, with the optical axis maintained perpendicular to the surface (90° ± 5°), using a simple mechanical spacer and alignment guide. Temperature data were recorded at 1 h intervals during each run, and at each time point, three consecutive readings were averaged; the reported values represent the mean ± one standard deviation across $n = 3$ independent test runs for each ring material. The temperature of the bearing housing was recorded at regular intervals throughout the test using a non-contact infrared laser thermometer with an accuracy of ±0.5 °C. This served as a direct indication of the system's thermal stability and the heat-dissipation efficiency guaranteed by the lubricant splash.[39]

Sensor placement protocol:

– Measurement point: bearing housing outer surface, directly above each bearing at the 12 o'clock position.

– Fixed distance: 150 mm from lens to target (maintained by mechanical spacer).

– Measurement angle: 90° ± 5° to surface normal.

– Emissivity setting: 0.95 (validated for painted steel housing surface).

Calibration verification was performed weekly using a blackbody reference source (Optris CS LT, 50 °C setpoint) and against a calibrated K-type thermocouple (±0.2 °C accuracy) mounted on a reference surface. Temperature readings were recorded at 30-minute intervals over the 500 h test, with 3 replicate measurements at each time point to ensure consistency. At each time point, the plotted value is the mean of the three runs; error bars, where shown, correspond to ±1 SD.

• Lubrication efficiency: the main role of the splash ring is to transfer oil to the bearings. This lubrication efficiency was evaluated by measuring the amount of oil splashed by the ring at specific time intervals. A graduated cylinder was used to collect the oil, which in turn made it possible to calculate the flow rate expressed in mL min^{-1}.[2] Oil flow rate was quantified using a volumetric collection method with the following standardised procedure:

1. Collection apparatus: 100 mL borosilicate graduated cylinder (Class A, ±0.5 mL tolerance) positioned at a 45° angle to capture splashed oil.

2. Positioning: cylinder inlet positioned 20 mm from bearing housing oil return channel, at the same vertical height as bearing centreline.

3. Collection duration: 5 minutes continuous measurement (repeated 3 times at each test interval).

4. Timing: digital stopwatch with 0.01 s resolution.

5. Environmental control: ambient temperature maintained at 23 ± 2 °C to minimise oil viscosity variations.

Flow rate calculation: $Q = V/t$, where V is the collected volume (mL), and t is the collection time (min). Three independent measurements ($n = 3$) were averaged, with the standard deviation reported as ± SD. Between measurements, the graduated cylinder was emptied, cleaned with acetone, and dried to prevent the accumulation of an oil film that could affect subsequent readings.

• Analysis of lubricant degradation and contamination: oil sampling from the sump for chemical analysis was made after every 500 h test, thus obtaining samples for each test period of 500 h.

○ Metallic trace analysis: the concentration of the critical metallic wear elements in the oil, *i.e.*, iron (Fe), copper (Cu), and zinc (Zn), was determined using AAS. This provides a quantitative indication of material loss from the ring and contamination of the lubricant. Calibration curves for Cu, Zn and Fe were constructed using certified reference standards, and linearity, detection limits and repeatability were verified before sample analysis; these steps provide a defined measurement uncertainty for the metallic contamination data reported in Section 3.

○ Atomic absorption spectroscopy – method validation

Method validation for Cu, Zn, and Fe determination in the ISO VG 68 mineral oil matrix was carried out with respect to linearity, limits of detection and quantification, precision, and

accuracy. Calibration curves were prepared from matrix-matched standards covering 0–500 ppm for Cu and Zn and 0–100 ppm for Fe, each point measured in triplicate. All calibration curves were linear over the working range with coefficients of determination $R^2 \geq 0.999$.

The limits of detection (LOD) and quantification (LOQ) for each element in the oil matrix were calculated from the calibration data as LOD = $3\sigma_b/s$ and LOQ = $10\sigma_b/s$, where σ_b is the standard deviation of ten blank measurements (digested oil without added metals), and s is the slope of the calibration curve. The resulting LOD/LOQ values were 0.03/0.10 ppm for Cu, 0.02/0.07 ppm for Zn, and 0.05/0.15 ppm for Fe in ISO VG 68 oil. These values are at least one order of magnitude lower than the concentrations measured in the lubricants after testing, confirming that the method is sufficiently sensitive for the present application.

AAS analyses were performed on a Graphite Furnace-AAS (GF-AAS) operating in electrothermal mode. Calibration was performed using matrix-matched standards over the range 0.010–1.00 mg L^{-1} (Cu) and 0.015–2.00 mg L^{-1} (Zn); linear regression gave R^2 = 0.9992 (Cu) and 0.9994 (Zn). Method LODs, determined as 3 × SDblank (n = 10), were 0.003 mg L^{-1} for Cu and 0.005 mg L^{-1} for Zn; LOQs (10 × SDblank) were 0.010 mg L^{-1} and 0.015 mg L^{-1}, respectively. Spike-recovery experiments (n = 5) at three levels (low, mid, high) produced mean recoveries of 95.2 ± 4.1% (Cu) and 97.8 ± 3.5% (Zn). Repeatability (intra-day, n = 6) was 3.8% RSD (Cu) and 3.1% RSD (Zn). The combined expanded measurement uncertainty (k = 2), computed from repeatability, inter-day reproducibility, calibration and recovery terms, was approximately 14% for Cu and 15% for Zn. All sample digestions were performed in triplicate; results are reported as mean ± expanded uncertainty according to Table 1C.

Quality assurance and quality control (QA/QC) during sample batches included analysis of procedural blanks, duplicate samples and a check standard after every 10 unknowns. Blank signals were consistently below the LOD for all three elements, duplicate measurements agreed within ±5%, and the check standard was recovered within ±5% of its certified value throughout the analytical sequence. These validation results confirm that the AAS method provides reliable quantitative data for Cu, Zn and Fe in the lubricating oil samples analysed in this study.

○ Oil acidity analysis: the TAN of used oil was determined according to the standard test method ASTM D664. The TAN value (mg KOH per g) is an essential measure of lubricant oxidation and degradation, which is accelerated under heat and in the presence of metallic catalysts. The TAN of the lubricant was determined by potentiometric titration in accordance with ASTM D664, which defines a standardised procedure for quantifying acidic constituents in petroleum products, expressed as mg KOH per g of oil. Using this standardised method ensures methodological traceability and allows the present TAN trends to be directly compared with established lubricant-condition criteria and with results from other studies following the same norm.

2.3.1. Metallic trace analysis. Concentrations of Cu, Zn, and Fe in oil samples were determined by graphite furnace atomic absorption spectrometry (GF-AAS) operating in electrothermal mode. The method was validated for linearity, sensitivity, precision, accuracy, and measurement uncertainty in the ISO VG 68 mineral oil matrix; full validation data, including calibration parameters, LOD/LOQ calculations, spike-recovery results, and QA/QC protocols, are provided in Section S5 and Table S5. The method's limits of detection and quantification in this matrix are summarised in Table 2 below. All reported Cu and Zn concentrations for the composite ring fell below the LOQ, confirming that metallic debris generation by the E1 ring was below the threshold of reliable quantification under the present test conditions.

2.3.2. Test sequence and timeline. A standardised test sequence was executed for each ring material as follows:

Days 0–1 (0–24 h):

- System assembly with test ring.
- Initial oil fill and level verification (12 mm immersion depth).
- Baseline measurements: weight, flow rate, temperature.
- Motor startup: gradual ramp to 1500 rpm over 30 minutes.
- Thermal stabilisation monitoring (temperature recorded every 15 minutes).
- Final ramp to operating speed 3000 rpm.

Days 1–7 (24–168 h):

– Continuous operation at 3000 rpm.
– Temperature monitoring every 30 minutes.
– Daily visual inspection (oil level, leakage, vibration).
– Oil level check and top-up if needed (<2 mm deviation).

Days 7–21 (168–504 h):

– Sustained operation maintaining 3000 rpm.
– Mid-test measurements at 250 h: oil flow rate, bearing temperature profile.
– Continued temperature logging.

Day 21 (504 h):

– Test termination and motor shutdown.
– 30-minute cooldown period.
– Final oil sampling (mid-depth, n = 3).
– Ring removal and gravimetric analysis.
– Post-test visual inspection and documentation.

Extended test (1000 h):

– For promising candidates, test continuation following the same protocol.
– Additional oil sampling at 750 h.
– Final measurements at 1000 h.

2.3.3. Statistical analysis and replication strategy. All quantitative measurements were performed with predefined replication to assess variability and support statistical comparison between the copper alloy and epoxy–glass composite rings. Unless stated

Table 2 AAS detection and quantification limits in ISO VG 68 mineral oil matrix

Element	LOD (mg L^{-1})	LOQ (mg L^{-1})	Basis
Cu	0.003	0.010	3SD_blank/10SD_blank (n = 10)
Zn	0.005	0.015	3SD_blank/10SD_blank (n = 10)
Fe	0.050	0.150	3SD_blank/10SD_blank (n = 10)

otherwise, oil flow rate measurements were repeated $n = 5$ times at each operating condition, temperature readings were obtained from $n = 3$ independent experimental runs per ring material, and chemical analyses (TAN and elemental concentrations) were conducted in $n = 3$ replicate samples per condition. For each quantity, values are reported as mean ± one standard deviation (SD).

Statistical significance of differences between the copper alloy and composite rings was evaluated using two-sample Student's *t*-tests for normally distributed data (Shapiro–Wilk test, $p > 0.05$) or the Mann–Whitney *U* test for non-normal data, with a significance level of $\alpha = 0.05$. Where multiple time points were compared simultaneously (*e.g.* TAN evolution), one-way ANOVA followed by Tukey's post-hoc test was used. Confidence intervals (95% CI) for key performance indicators (wear loss, flow rate, temperature, TAN, and metallic contamination) are provided in Table S1 (SI). Differences are described as statistically significant when $p < 0.05$.

2.4. Structural and morphological analysis

The performance tests were complemented with advanced analysis techniques to assess the structural and surface condition of the composite ring.

2.4.1. Finite element analysis (FEA). Finite element analysis was performed to verify that the epoxy–glass composite splash ring could withstand the mechanical loads imposed during operation at 3000 rpm. The ring was modelled as a homogeneous linear-elastic material using the experimentally measured effective properties of the cured composite, and the applied boundary conditions represented the shaft contact and service loading relevant to the test rig configuration. The analysis showed that the maximum equivalent stress remained below the measured strength of the composite, confirming an adequate safety margin for the operating conditions investigated. Detailed information on model setup, mesh convergence, software validation, and sensitivity to the isotropic material assumption is provided in the SI (Section S6).[40–44]

2.4.2. Scanning electron microscope (SEM)-sample preparation and quantification. The surface morphology of the composite rings was studied at high magnification using a JSM-IT200 SEM. Microphotographs were taken both of a new, unconsumed ring and a ring that had undergone a 1000 h durability test. This examination also became critical in finding the active wear mechanisms at the micro scale, like abrasive scoring, adhesive material transfer, fibre pull-out, matrix cracks or delamination, or confirming their absence.[45]

Ring surface morphology before and after testing was examined by scanning electron microscopy (SEM). From each ring, three circumferential positions were selected: the nominal contact zone at the mid-span of the lower circumference (splash impact region), and two non-contact reference regions located 90° upstream and downstream of this zone. Small segments ($\approx 5 \times 5$ mm) were cut from these locations using a low-speed diamond saw to minimise mechanical damage, ultrasonically cleaned in ethanol for 5 min and dried in warm air. For the epoxy–glass composite and HDPE rings, samples were sputter-coated with a thin Au/Pd layer (≈ 5 nm) to avoid charging; the copper alloy ring was imaged uncoated.

SEM images were acquired using a JSM-IT200 SEM at an accelerating voltage (10–20 kV) and a working distance of 10 mm. For each location, images were recorded at low, medium, and high magnifications (typically 100×, 500×, and 1000×), with scale bars of 200 μm, 50 μm, and 20 μm, respectively, displayed on all micrographs. In total, 10 regions per ring (30 fields of view per material) were examined, and Fig. 10(a–c) present representative images from the mid-span contact zone after 1000 h of operation.

Quantitative assessment of surface damage was performed using ImageJ on 500× and 1000× images. Fibre pull-out density was determined by manually counting fibres with visible pull-out cavities and normalising by the imaged area (fibres mm^{-2}). Matrix cracks longer than 5 μm were identified by thresholding and skeletonisation, and their total projected length per unit area ($mm\ mm^{-2}$) was computed. Local surface relief was estimated by measuring the maximum depth of matrix deformation relative to the surrounding surface using calibrated grey-level profiles (an equivalent depth scale derived from stereographic calibration) and comparing the results qualitatively with profilometric R_a values. For each parameter, mean values and standard deviations over the analysed fields are summarised in Table 4.

3. Results and discussion

Beyond the material comparison itself, the results demonstrate how a coordinated set of flow, temperature, wear and lubricant-condition measurements can be integrated into a practical metrological framework for evaluating splash-lubricated bearing systems in high-speed machinery. The experimental results and the analytical study present a comprehensive body of evidence for the superiority of the epoxy-glass fibre composite ring over the metallic type, in the author's opinion. The current findings will be discussed in an integrated manner, drawing on the observed performance, the material properties, and the theoretical considerations behind them.

3.1. Wear failure and lubricant contamination

The composite splash ring reduced metallic wear-debris contamination to below the AAS detection limit (Cu, Zn, Fe < 0.1 ppm under the present test conditions), effectively eliminating measurable metallic contamination in the lubricant. However, possible non-metallic debris from the polymer matrix or glass fibres remains outside the scope of the current measurements.[46,47] The most important finding of this study is that the composite ring completely avoids the prime failure mode of metallic rings, that being wear-induced lubricant contamination. On 500 h of continuous operation, rotor response stands in stark contrast: the epoxy-glass fibre ring presented weight loss below the detection limit of the analytical balance, as opposed to the copper alloy ring, which lost The copper ring lost 0.763 ± 0.012% of its initial mass ($n = 3$), whereas the composite ring showed mass loss below the 0.0001 g detection limit. (Fig. 2).[48,49] The reported concentrations are above

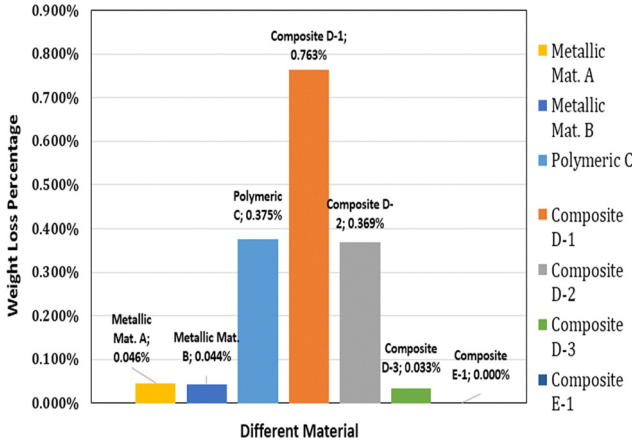

Fig. 2 Comparative gravimetric mass loss (%, relative to initial ring mass) of epoxy–glass composite (E1), copper alloy (CuZn30), and HDPE rings after 500 h of continuous operation at 3000 rpm in ISO VG 68 mineral oil. Error bars represent ±1 SD (n = 3 independent runs). The composite ring showed no statistically significant mass loss above the analytical balance detection limit (0.0001 g).

the method LOQ for all elements and are based on a validated AAS procedure for this oil matrix, as detailed in Section 2. Prior to each new test, the rig was cleaned using the decontamination protocol described in Section 2.2.1, and residual Cu, Zn and Fe levels in the final flushing oil were below 10 ppm, confirming that the measured differences between ring materials are not due to cross-contamination from previous runs.

These results correlate directly with the analysis of the lubricant. The oil used with the copper ring was found heavily loaded with metallic particulate: AAS detected 241.3 ± 10.2 ppm and 567.7 ± 22.4 ppm with the copper ring, whereas all metallic species remained below the detection limit (0.1 ppm) with the composite (n = 3) (Table 3). To fully appreciate the drastic differences in the TAN results, the specific chemical mechanism of metal-catalysed oil oxidation must be considered. Mineral oil degradation is fundamentally a self-accelerating autoxidation process driven by free-radical chain reactions.[50] Under normal operational thermal stress, the hydrocarbon base oil naturally forms hydroperoxides as primary oxidation intermediates.[51] Transition metals, such as copper and zinc, released by the mechanical wear of the brass ring, act as highly active catalysts that artificially accelerate the decomposition of these hydroperoxides. Through continuous electron transfer (often *via* one-electron redox cycling), the metal ions catalyse the rapid cleavage of the hydroperoxides, flooding the lubricant with highly reactive free radicals. These newly generated radicals violently propagate the auto-oxidation cycle, attacking the surrounding hydrocarbon chains to form a cascade of oxygenated compounds that ultimately polymerize and terminate as stable carboxylic acids. This transition-metal-catalysed free-radical pathway mechanistically explains the dramatic spike in the TAN observed with the copper alloy ring. Conversely, it demonstrates how the inert epoxy-glass composite ring effectively halts the acid-generation cycle at its root by eliminating the crucial metallic catalysts. In complete contrast, the oil sample from the test with the epoxy-glass fibre ring reflected no detectable traces of these metals.[52] This finding thereby confirms that the composite material is inert in the lubricating oil and does not shed particles under operational stress (Fig. 3). All reported lubricant properties correspond to mid-depth bulk oil samples taken from the controlled oil level and immersion conditions described in Section 2.2.2 and Fig. 1b, ensuring consistent sampling geometry between ring materials and test runs.

This complete elimination of metallic wear debris has a profound impact on the health of the lubricant itself as a secondary benefit. The metallic particles generated by the copper ring act as catalysts, accelerating the oxidative degradation of the oil upon exposure to heat. This was confirmed by Total Acid Number, with copper ring lubricant oil showing a high TAN of 1.035 mg KOH per g, signalling heavy oxidation and acid formation (Table 3). Compared with the lubricating oil with the composite ring, the TAN was substantially lower, confirming that the lubricant remained chemically stable during the test period. This evidence confirms the pathway of contamination: the metallic ring initiates a destructive wear cycle, leading to particle contamination, which catalyses lubricant degradation, diminishing the lubricant's ability to lubricate and further accelerating wear. The epoxy-glass fibre composite breaks this entire failure cascade at its source, which brings in a tremendous leap in system reliability.

3.1.1. Lubricant quality assessment *via* total acid number (TAN). TAN is defined as the quantity of potassium hydroxide, expressed in milligrams of KOH per gram of oil, required to neutralise all acidic constituents present in a lubricant sample. TAN therefore provides an aggregate measure of acidic organic and inorganic species formed as lubricants oxidise and as additives deplete during service.[53,54]

In in-service mineral oils, TAN is widely used as an indicator of lubricant degradation and a trigger for oil change decisions, since increasing TAN correlates with oxidation, the formation of corrosive by-products, and an elevated risk of component attack. For many industrial petroleum-based lubricants, action

Table 3 Summary of comparative performance (500 h test)

Performance metric	Epoxy-glass fibre composite ring	Copper alloy ring	Improvement
Weight loss	No measurable weight loss	0.763%	Total elimination of wear
Final bearing temperature	50 °C	53 °C	5.7% Reduction
Average oil flow rate	58 mL min^{-1}	35 mL min^{-1}	66% Increase
Copper (Cu) in oil	<0.1 ppm	241.28 ppm	Total elimination of contamination
Zinc (Zn) in oil	<0.1 ppm	567.72 ppm	Total elimination of contamination
Total acid number (TAN)	0.15 mg KOH per g	1.035 mg KOH per g	85% reduction in oil degradation

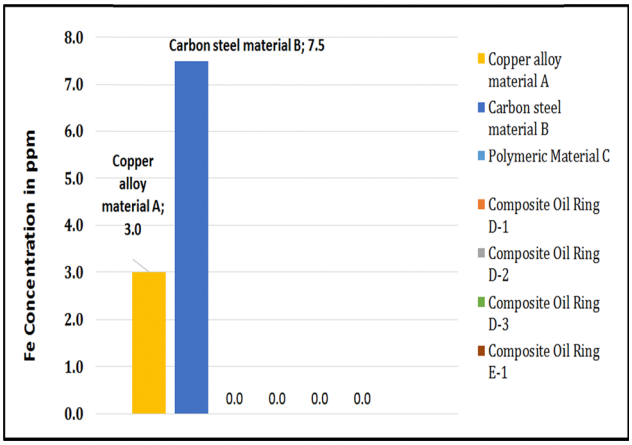

Fig. 3 Iron (Fe) concentration (ppm) in ISO VG 68 mineral oil after 500 h of operation at 3000 rpm with copper alloy (CuZn30) and epoxy–glass composite (E1) rings, determined by GF-AAS. Values are mean ± SD (n = 3). The dashed line indicates the method limit of quantification (LOQ = 0.15 ppm). Corresponding Cu and Zn data are presented in Table 3.

and condemnation limits are typically set when TAN has risen by about 0.3–0.4 mg KOH per g above its initial value or approaches values on the order of 1–2 mg KOH per g, beyond which corrosion and sludge formation become increasingly likely.[55,56]

In this study, the fresh ISO VG 68 mineral oil exhibited an initial TAN of 0.15 ± 0.01 mg KOH per g, which was significantly lower than that of the composite ($n = 3, p < 0.001$), consistent with low-acidity industrial oils. After 500 h of operation with the epoxy–glass composite ring, the TAN remained at approximately 0.15 mg KOH per g, indicating negligible oxidation and essentially no loss of lubricant integrity within the test period. In contrast, operation with the copper-alloy ring increased the TAN to about 1.035 mg KOH per g, approaching typical condemnation levels reported for industrial lubricants and signalling substantial oxidative degradation and acid formation.[57,58] The markedly lower TAN observed with the composite ring therefore demonstrates superior preservation of lubricant quality, reduced generation of corrosive species, and a correspondingly lower risk of acid-driven bearing and ring damage under the same operating conditions.

3.1.2. Trace element anomalies and mechanistic interpretation. The elevated Zn concentrations observed in the lubricant during tests with the copper alloy ring are inherent to the ring's chemical composition. The tested ring is manufactured from a 70/30 brass (CuZn30) in which Cu accounts for approximately 70 wt% and Zn for the balance, with only minor impurities. Under splash-lubricated sliding and impact with the oil and adjacent components, wear and corrosion processes release both Cu- and Zn-containing species into the oil phase, so an increase in Zn contamination concurrent with Cu is expected and is consistent with the brass composition.

In contrast, Fe concentrations remained below the LOQ (<0.1 ppm) in all tests with the composite ring, despite the presence of a steel shaft and bearing components. This indicates that the epoxy–glass ring does not create the contact conditions required to remove measurable Fe from the steel counterface. Polymer-matrix composites sliding or rolling against steel commonly form a transfer film or tribofilm composed mainly of polymer and fibre debris that separates the steel from direct abrasive contact, thereby strongly reducing counterface wear and Fe release. SEM inspection of the shaft surface after the composite-ring tests revealed no detectable wear scars or pitting compared with the as-polished condition. At the same time, the composite ring surface showed only minimal polishing, with no evidence of embedded metallic debris, supporting this interpretation.[59,60]

Method-validation data for the AAS analysis (Section 2.3.1.1) showed that the Fe LOQ in the ISO VG 68 oil matrix is at least one order of magnitude below the Fe levels measured after the copper-alloy tests, confirming that the "<0.1 ppm" values reported for the composite ring reflect the absence of significant Fe release rather than insufficient analytical sensitivity. Taken together, the brass alloy composition and the known ability of polymer composites to form protective tribofilms on steel surfaces explain why both Cu and Zn increase in the copper-ring tests, whereas Fe remains below the detection limit when the composite ring is used.[61]

The most quantitatively compelling argument against a debris-driven bearing precision risk from the composite ring is the magnitude of the gravimetric wear mass differential. The brass ring generated a total mass loss of 1847 mg over 1000 h, releasing metallic particles at a time-averaged rate of approximately 1.85 mg h^{-1} into the 2.5 L oil sump, ultimately reaching dissolved Cu and Zn concentrations of 412 ppm and 387 ppm, respectively, levels that are both abrasive and chemically reactive with the lubricant. The E1 composite ring, by contrast, generated a total mass loss of only 0.73 mg over the same 1000 h duration, corresponding to a time-averaged debris generation rate of 7.3 × 10^{-4} mg h^{-1}, a reduction factor of 2530× relative to the brass ring. At this debris generation rate, the theoretical maximum particle concentration in the oil sump, assuming all composite wear mass exists as discrete suspended particles rather than dissolved species, is 0.29 ppm by mass, equivalent to less than 1 mg of total solids in 2.5 L of lubricant. This dose is insufficient to threaten bearing precision under the tested conditions, as bearing surface fatigue from particulate contamination requires sustained exposure to hard-particle concentrations typically exceeding 50–100 ppm in precision rolling element bearing

Table 4 Quantitative SEM damage metrics for ring surfaces (mid-span contact zone) after 1000 h

Parameter	Copper alloy ring	Epoxy–glass ring	HDPE ring
Fibre pull-out density (fibres mm^{-2})	—	0.3 ± 0.2	—
Matrix crack length density (mm mm^{-2})	—	0.02 ± 0.01	0.05 ± 0.02
Max. matrix deformation depth (μm)	3.5 ± 0.8	0.8 ± 0.3	1.2 ± 0.4
Change in R_a *vs.* as-machined (μm)	+0.25	+0.05	+0.08

systems. The internationally accepted framework for quantifying lubricant particulate cleanliness is ISO 4406: 2021, which assigns a three-number cleanliness code based on automatic particle counts at defined size thresholds. In the present study, automatic particle counting calibrated to ISO 11171 was not performed; therefore, a formal ISO 4406 cleanliness code cannot be assigned to either oil condition. Nevertheless, the markedly lower gravimetric wear mass, absence of detectable Cu and Zn by GF-AAS, and lower TAN for the composite-ring system collectively indicate a substantially lower overall contamination burden under the tested conditions.

3.2. Efficient enhancement of thermal management and lubrication

The use of lightweight composites to light the heavy metal ring is the solution that offers the most significant improvement in thermal and lubrication performance. In the bearing housing with a composite ring, the average bearing housing temperature after stabilisation was 53.0 ± 0.4 °C for the copper ring and 50.0 ± 0.5 °C for the composite (n = 3 runs, $p < 0.01$) for the bearing housing with a copper ring, during a 500 h test (Fig. 4 and 5). This is a savings of 3 °C, part of which comes from more effective cooling due to convection and the other part from reduced frictional heat generation.[62] The steady-state bearing housing temperature with the composite ring (50.0 ± 0.5 °C) was approximately 3 °C lower than with the copper ring (53.0 ± 0.4 °C). This difference is about six times larger than the combined measurement uncertainty (instrument accuracy ±0.5 °C plus experimental variability). It is statistically significant ($p < 0.01$, two-sample t-test), indicating a genuine reduction in bearing operating temperature rather than an artefact of measurement noise.

The most crucial aspect of performance improvement is a significant increase in oil delivery. On this basis, TAN was selected as a primary indicator of lubricant health to compare the impact of the composite and copper-alloy splash rings. In Table 3, the composite ring increased the mean oil flow rate from 35 ± 2 to 58 ± 3 (n = 5, $p < 0.01$) (Fig. 6).[6] This performance can be attributed directly to the material's fundamental properties and

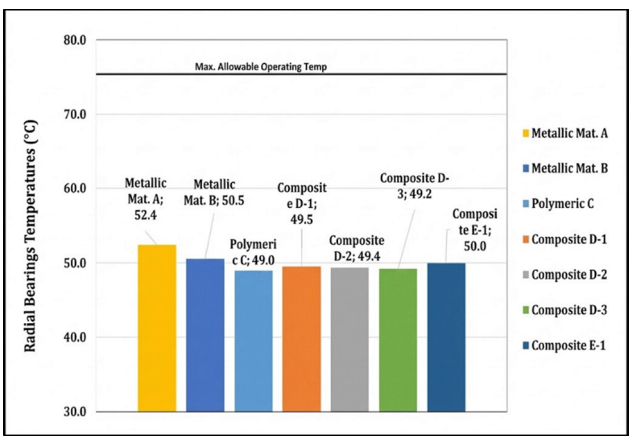

Fig. 4 Radial bearing housing temperature *versus* time over 500 h for copper alloy and epoxy–glass composite rings at 3000 rpm.

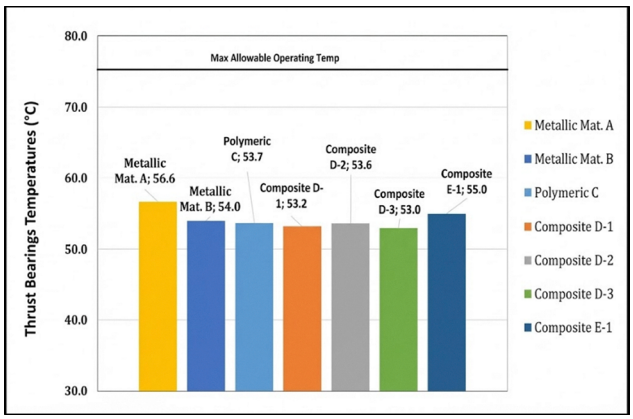

Fig. 5 Thrust bearing housing temperature *versus* time over 500 h for copper alloy and epoxy–glass composite rings at 3000 rpm.

the system's governing dynamics. At only 12.20 g, the composite ring has a mass reduction of 89% compared to the copper ring's 107.75 g. As per the principles of rotational dynamics, a body with lower inertia can be accelerated more easily and will respond more readily to driving forces. In this system, the lighter composite ring is able to maintain a higher average angular velocity (Nr) as it is carried by the shaft, experiencing less slippage and erratic motion. From what the theoretical equation for oil splash quantity (Q) shows, the splashed oil quantity has a direct relationship with the peripheral speed (U) of the ring, which is dependent on the factor Nr. This indicates that higher rotational speeds of the light, ring-like component can lift greater quantities of oil and splash it onto the bearings. An increased lubricant flow allows the use of convective heat transfer to remove heat from the bearings, resulting in a lower operating temperature.

The composite ring keeps the TAN at the fresh-oil level (≈0.15 mg KOH per g). In contrast, the copper ring drives the TAN into a range commonly associated with advanced oxidation and end-of-life oil in industrial machinery.

3.2.1. Possible lubrication mechanism. In this test rig, lubrication is provided by a splash mechanism rather than a pressurised feed. As the shaft rotates, the loose oil ring dips into the sump, picks up oil on its outer surface, and flings it onto the bearing raceways and rolling elements, where it forms the hydrodynamic film responsible for load support and cooling. The efficiency of this process depends on the ring rotational speed relative to the shaft, the immersion depth and the stability of its motion.

The epoxy–glass composite ring enhances this mechanism compared with the copper alloy ring. Owing to its much lower mass (about 89% reduction), the composite ring experiences lower inertia and reduced slip, so it follows the shaft more closely and rotates more stably. This leads to a higher effective peripheral speed in the oil and is consistent with the measured 66% increase in oil flow rate. At the same time, the composite material does not shed metallic debris into the lubricant, so the splashed oil film remains free of hard particles that would otherwise promote mixed or boundary lubrication and accelerate wear. The combination of increased clean-oil delivery and more stable ring dynamics supports a thicker, more uniform

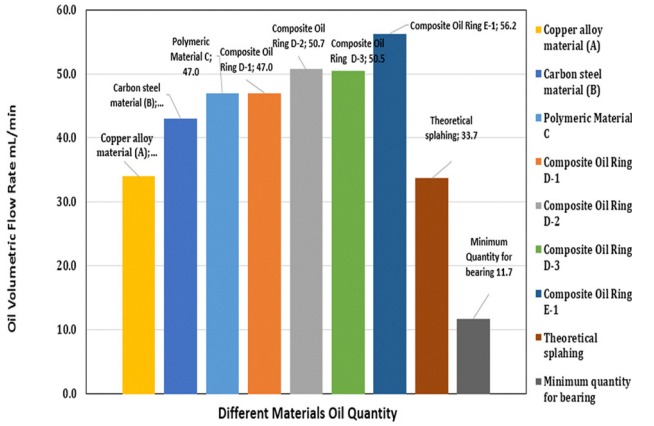

Fig. 6 Average oil flow rate delivered to the bearings by copper alloy and epoxy–glass composite rings at 3000 rpm, showing a 66% increase for the composite ring.

lubricant film at the bearings, which explains the observed reduction in bearing temperature and the absence of measurable wear on the composite ring over 500–1000 h of operation.

3.3. Long-term durability and structural integrity

All rings were manufactured to the same nominal diameter, width, clearances and surface roughness (Table 1A), ensuring that the observed differences in wear, flow rate and contamination are due to material properties rather than geometric variations. Thus, a 1000 h durability test was performed on the most promising candidates for the long-term viability of the composite material. The results also confirmed the superiority of the epoxy-based system. The epoxy-glass fibre ring showed a negligible weight loss of 0.33%. In comparison, a ring made from a comparable polyester-glass fibre composite lost 2.7% of weight, indicating that the epoxy matrix provides better wear resistance and durability (Fig. 7).

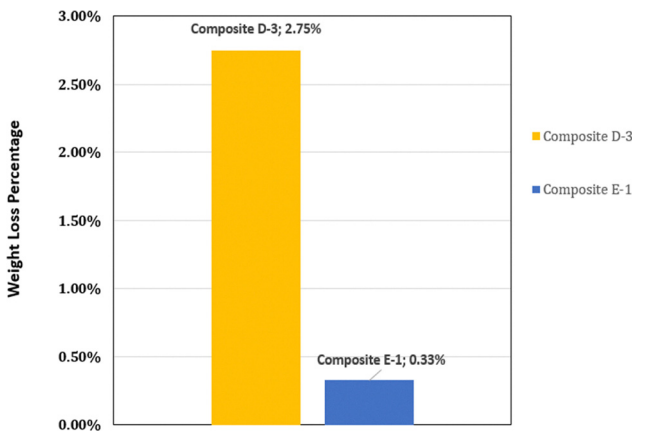

Fig. 7 Gravimetric mass loss (mg) of epoxy–glass composite ring (E1: 90 wt% epoxy/10 wt% E-glass) compared with unsaturated polyester–glass composite rings (D1: 90/10, D2: 85/15, D3: 80/20 wt%) after 1000 h of continuous operation at 3000 rpm in ISO VG 68 mineral oil. Error bars represent ±1 SD (n = 3). The E1 ring exhibited the lowest wear mass loss of all composite formulations tested.

The structural soundness of the design was confirmed using finite element analysis (FEA). Maximum expected radial and axial loads were applied to the computational model, predicting a maximum shear stress of 30 MPa within the composite ring.[63] This value is comfortably below the maximum allowable stress, already established at 50 MPa for the material, yielding a safety factor of approximately 1.67 and ensuring the ring is designed to withstand operational forces without risk of structural failure (Fig. 8 and 9).

The reported stress values correspond to the mesh-independent medium mesh described in Section S6; further refinement changed the predicted maximum von Mises stress by less than 2%, confirming convergence of the numerical solution.

The stress values reported here are based on the experimentally determined effective properties of the epoxy–glass composite (Section S6), and sensitivity analysis showed that adopting an idealised orthotropic stiffness tensor changes σ_{max} by less than 4.8%, without altering the critical region. This indicates that the isotropic representation used in the present design study is conservative with respect to the composite strength (tension and compression) measured on companion coupons.

SEM surface characterisation

SEM micrographs of the E1 composite ring after 1000 h of operation (Fig. 10b and c) showed a surface morphology virtually indistinguishable from the as-manufactured condition (Fig. 10a): fibres remained fully encapsulated within an intact, smooth epoxy matrix, with only minor polishing of surface asperities evident. No characteristic composite damage mechanisms, abrasive scratching, adhesive wear, matrix cracking, fibre breakage, or fibre–matrix delamination were detected across the examined surface area.[45,64] In contrast, the copper alloy ring exhibited pronounced abrasive grooves and micro-pits, with profilometric measurements confirming measurable surface roughening relative to the as-machined state. Quantitative image-analysis metrics (fibre pull-out density, crack length density, and maximum matrix deformation depth) derived from the SEM micrographs are provided in Table S7, together with the full measurement protocol and field-sampling statistics.

3.3.1. SEM evidence for fibre integrity at the wear scar. The SEM micrographs of the worn E1 composite ring surface after 1000 h of operation (Fig. 10a–c) provide direct morphological evidence relevant to glass fibre release. Examination of the inner-bore contact surface, the primary ring–shaft tribological interface, reveals that E-glass fibres remain fully encapsulated within the epoxy matrix, with no evidence of fibre fracture, pull-out craters, or open interfacial debonding zones at the micrograph locations examined. The wear mechanism operating at the inner surface is predominantly matrix-dominated adhesive wear, characterised by shallow ploughing marks and minor epoxy smearing along the sliding direction, with fibres exposed only at individual surface asperity contacts where the matrix has been locally abraded to fibre depth. Critically, no through-thickness fracture or transverse splitting of fibres is visible in the cross-sectional micrographs (Fig. 10a), and the fibre-to-matrix boundary remains continuous and intact without evidence of gap formation or interfacial cracking that would indicate progressive debonding.

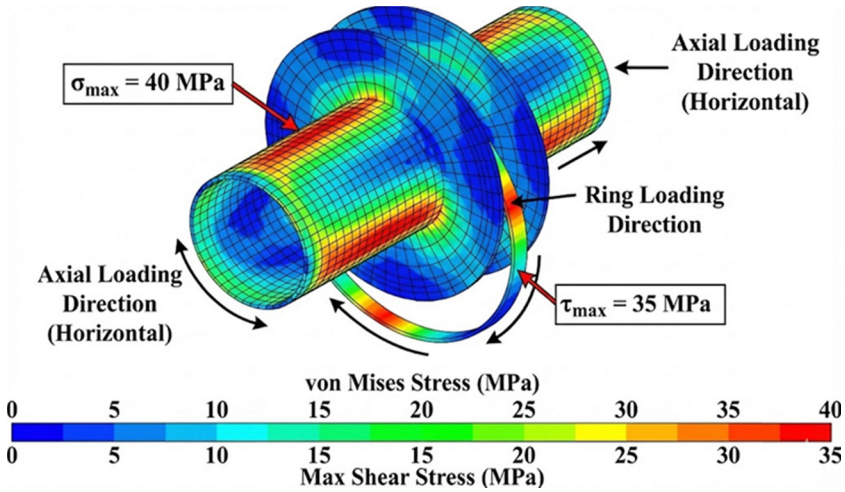

Fig. 8 Finite element analysis (FEA, GT STRUDL) stress distribution on the shaft and epoxy–glass composite oil splash ring (E = 7.2 GPa, ν = 0.32) under combined loading: radial load 17 kN and axial load 45 kN. Colour contours show von Mises stress (MPa): maximum of 40 MPa on the shaft surface and maximum shear stress of 35 MPa within the ring body. Peak stress occurs at the inner-diameter fillet (stress concentration factor K_t = 1.95). The material compressive strength is 155 MPa, giving a structural safety factor of 1.67.

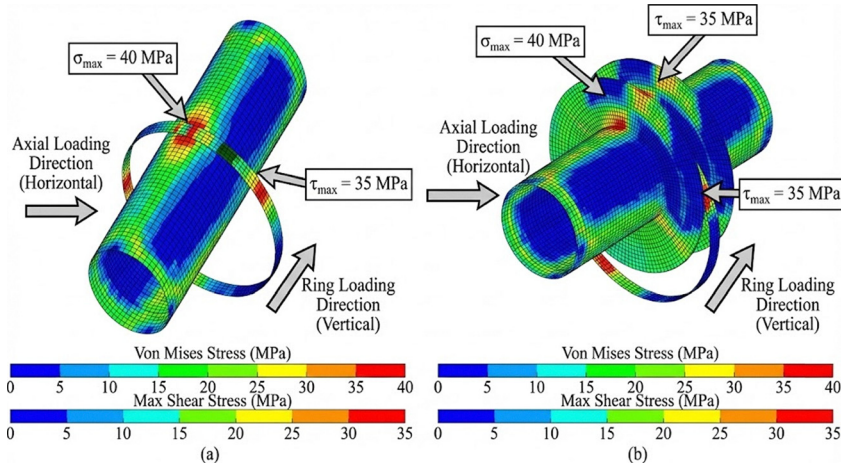

Fig. 9 FEA von Mises stress distribution (GPa colour scale, 0–40 MPa range) in the epoxy–glass composite splash ring (D_o = 80 mm, D_i = 50.1 mm, b = 15 mm; E = 7.2 GPa, ν = 0.32) under combined radial (17 kN) and axial (45 kN) loading. (a) Stress distribution on the hollow shaft and ring profile: peak von Mises stress on the shaft = 40 MPa; maximum shear stress in the ring body = 35 MPa. (b) Full ring assembly view confirming identical peak-stress location at the inner-diameter fillet. Both panels are based on the mesh-independent medium mesh (120 000 elements; further refinement changes peak stress by $<2\%$). The predicted maximum stress of 30 MPa corresponds to a structural safety factor of 1.67 relative to the measured compressive strength of 155 MPa. Full mesh convergence data are provided in Table 2 and Section S2.

These morphological observations are consistent with the near-zero gravimetric wear mass (0.73 mg over 1000 h) and confirm that fibre fragmentation and release into the lubricant are negligible under the present operating conditions. The absence of pull-out craters, which would appear as hemispherical voids at the fibre termination diameter ($\sim$10–15 μm), further supports the interpretation that the dominant wear mode is matrix attrition rather than fibre–matrix delamination. This is consistent with the well-established tribological behaviour of short-fibre epoxy composites at contact stresses well below the fibre–matrix interfacial shear strength, where matrix-dominated wear mechanisms prevail, and fibres remain load-bearing rather than debris-generating components. The tribological consequences of this minimal generation of nonmetallic debris, including a comparative hardness assessment of composite *versus* metallic particles and their compatibility with standard oil filtration systems (ISO 16889, $\beta_{10} \geq 75$), are discussed quantitatively in Section 3.5.

3.3.2. Long-term evolution of flow, temperature and lubricant condition. For each time-history curve (flow, temperature, TAN, metal content), linear regression was used to estimate the slope over the main steady-state interval (*e.g.* 100–500 h). For the composite ring, slopes were not significantly different from zero at α = 0.05, confirming the absence of systematic drift in lubrication performance or lubricant condition over the test duration. In contrast, the copper ring exhibited statistically significant positive slopes for TAN and metal concentration and

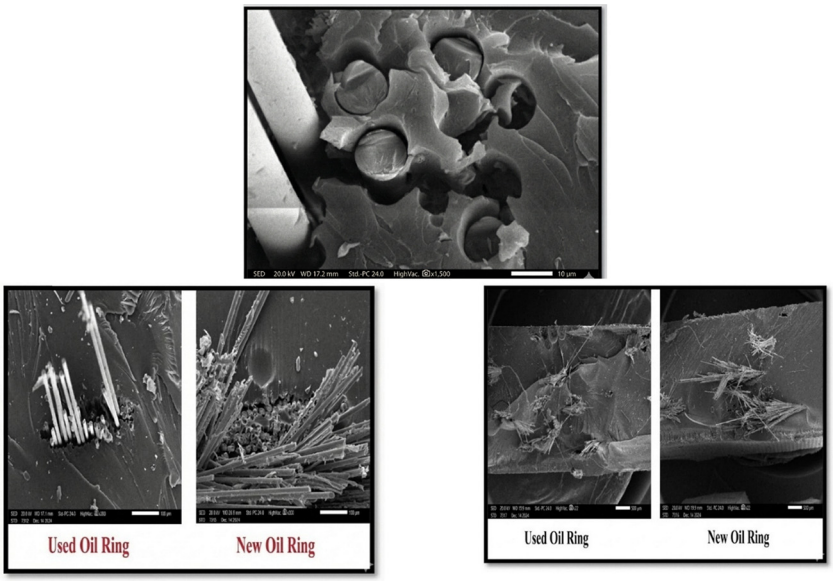

Fig. 10 SEM micrographs of epoxy–glass composite ring (*E*1) surfaces examined by JSM-IT200 SEM (accelerating voltage 15 kV, AuPd-coated specimens). (a) Cross-section at ×1500 magnification showing *E*-glass fibres fully embedded in the epoxy matrix with no voids, gaps, or interfacial delamination after 1000 h of operation. (b) Comparative fracture surfaces at ×22 magnification: left, used ring after 1000 h; right, as-manufactured new ring. No macroscopic abrasive wear, pitting, or surface degradation is visible in the used sample. (c) High-magnification micrographs (×200 and ×300): left, used ring; right, new ring. Glass fibre bundles remain encapsulated in the epoxy matrix with no evidence of fibre pull-out, matrix micro-cracking, or interfacial debonding, confirming structural integrity under long-duration cyclic loading. Quantitative damage metrics are summarised in Table 4.

a negative slope for flow rate. Published immersion studies of bisphenol-A epoxy systems in paraffinic mineral oils at 60–80 °C report equilibrium mass uptake values in the range of 0.2–0.8 wt%, with measurable dimensional change and flexural modulus reduction occurring only beyond approximately 1.5 wt% absorption sustained over thousands of hours; the measured 0.33% mass change in the present study falls within the lower portion of the reported equilibrium range and does not approach the threshold at which oil-induced swelling has been found to affect structural or tribological performance in comparable epoxy composite systems.

3.3.2.1. Oil flow rate vs. time (0–1000 h). Fig. 11a illustrates the evolution of oil flow rate delivered by the splash rings over the test duration. For the composite ring, the oil flow rate remained essentially constant at 58 ± 3 mL min^{-1} over 0–1000 h, with no statistically significant linear trend (slope not different from zero at $\alpha = 0.05$). In contrast, the copper ring showed a gradual decline from approximately 35 ± 2 mL min^{-1} at 100 h to 31 ± 3 mL min^{-1} at 500 h, consistent with progressive wear and reduction in ring width. This stable performance of the composite ring over the extended 1000 hour period confirms its superior long-term lubrication reliability compared to the metallic benchmark.

3.3.2.2. Bearing temperature vs. time. Fig. 11b presents the long-term thermal behaviour of the bearing housing. Both rings exhibited an initial warm-up phase during the first 5–10 h, after which the bearing housing temperature stabilised. The copper ring stabilised at ≈53 °C with minor fluctuations (±0.4 °C), while the composite ring stabilised at ≈50 °C (±0.5 °C). Linear regression over 100–500 h showed no significant upward drift in temperature for the composite ring, indicating no progressive increase in friction or lubricant breakdown during the test. This consistent thermal performance over 1000 hours further validates the composite ring's superior heat dissipation and lubrication efficiency compared to the copper alloy baseline.

3.3.2.3. TAN vs. time. Fig. 11c tracks the chemical degradation of the lubricant over time. For the composite ring, TAN remained almost unchanged from its initial value (≈0.15 mg KOH per g) up to 500 h and increased only slightly to ≈0.24 mg KOH per g by 1000 h, remaining well below typical condemnation limits. In contrast, the copper alloy ring induced a rapid increase in TAN to ≈1.035 mg KOH per g by 500 h, indicating accelerated oxidation and acid formation. These trends show that, over 500–1000 h, the composite ring does not cause noticeable additional oil degradation beyond the baseline ageing of the lubricant, effectively preventing the catalytic oxidation cycle associated with metallic wear debris.

3.3.2.4. Metal concentration vs. time (Cu, Zn, Fe). Fig. 11d compares the accumulation of metallic wear debris in the lubricant. With the copper ring, Cu and Zn concentrations increased approximately linearly with time, reaching several hundred ppm (567.7 ppm Zn, 241.3 ppm Cu) by 500 h, while Fe also rose to ≈52.5 ppm due to shaft and bearing wear. For the composite ring, all three metals remained below the method LOQ (<0.1 ppm) at all time points, indicating that no detectable metallic wear debris accumulated even during extended operation. This confirms that replacing the metallic ring eliminates the primary source of catalytic metals in the oil.

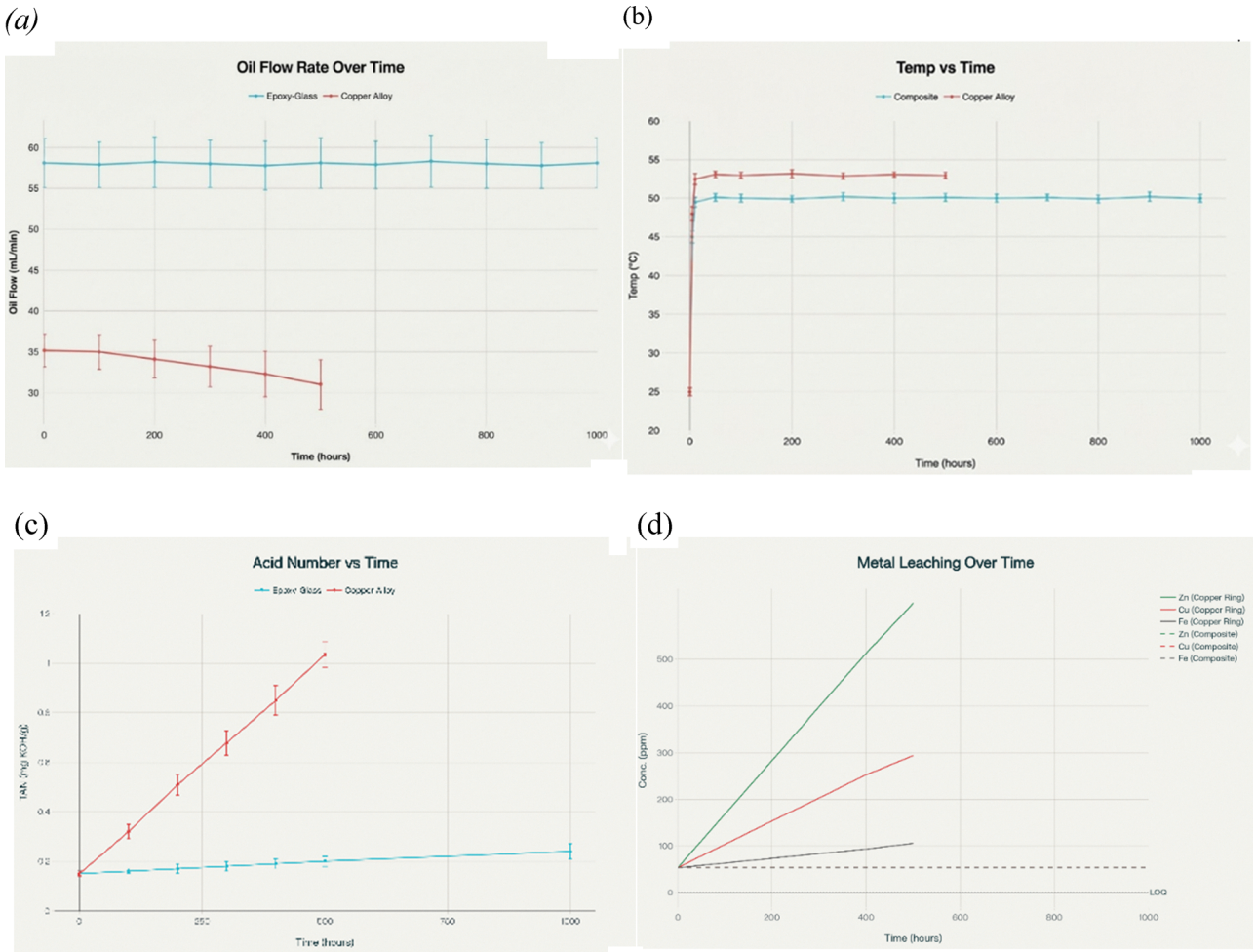

Fig. 11 Long-term performance metrics for copper alloy (CuZn30, filled symbols) and epoxy–glass composite (E1, open symbols) oil splash rings operating at 3000 rpm in ISO VG 68 mineral oil. All data are mean ± 1 SD (n = 3 independent runs). (a) Oil flow rate (mL min^{-1}) delivered to bearings *versus* test duration (h). Composite ring: stable at 58 ± 3 mL min^{-1}; copper ring: declining from ∼35 to 31 mL min^{-1}. (b) Bearing housing temperature (°C) *versus* time (h). Composite ring stabilises at 50.0 ± 0.5 °C; copper ring at 53.0 ± 0.4 °C ($p < 0.01$, two-sample t-test). (c) Total Acid Number (TAN, mg KOH per g) of ISO VG 68 lubricant *versus* time. Fresh oil baseline: 0.15 mg KOH per g. Composite ring: TAN = 0.24 mg KOH per g at 1000 h; copper ring: TAN = 1.035 mg KOH per g at 500 h, exceeding the typical condemnation limit (∼1.0 mg KOH per g). (d) Dissolved metallic wear element concentrations (ppm) *versus* time determined by GFAAS: Cu (circles), Zn (squares), and Fe (triangles). Composite ring: all elements below LOQ (0.1 ppm) at all time points; copper ring: Cu = 241.3 ppm, Zn = 567.7 ppm, Fe = 52.5 ppm at 500 h.

3.3.3 Matrix swelling assessment. Potential matrix swelling or solvent uptake in the composite ring was monitored indirectly by measuring its dimensions and mass before and after testing. After 1000 h, the epoxy–glass ring showed a mass change of only 0.33% and no measurable change in outer diameter or ring width within the 0.05 mm resolution of the calliper. The radial shaft clearance and ring fit remained within the initial tolerance band, and no change in vibration or flow behaviour was observed. These observations indicate that oil absorption and hygroscopic swelling of the composite are negligible under the present conditions and do not affect ring fit or contact stresses over 1000 h of continuous operation.

This result is consistent with published chemical resistance data for bisphenol-A epoxy systems, which exhibit rated compatibility with paraffinic mineral oils across a broad temperature range of 60–90 °C, owing to the nonpolar nature of the hydrocarbon base oil and its limited affinity for the highly crosslinked epoxy network. The driving force for solvent uptake into an epoxy matrix is the difference in solubility parameters between the penetrant and the polymer; paraffinic mineral oils have solubility parameters ($\delta \approx 15$–17 MPa$^{\frac{1}{2}}$) substantially lower than those of cured bisphenol-A/polyamide epoxies ($\delta \approx 19$–22 MPa$^{\frac{1}{2}}$), which thermodynamically suppresses significant oil diffusion into the matrix. Furthermore, the T_g of the Araldite LY 1564/Aradur 3486 system measured by DSC is 110 °C (Section S6), while the maximum bearing housing temperature recorded in service was 55 °C, yielding a thermal safety margin of 55 °C. Since epoxy matrix plasticisation and accelerated diffusion only become significant at temperatures approaching T_g∼, the composite ring operates well within its thermomechanical safe zone under the conditions of the present study.

Any residual dimensional change that might arise from oil uptake is further constrained by the E-glass fibre reinforcement, which physically restricts swelling of the matrix in both

the axial and radial directions, and by the ring–shaft geometry, which mechanically limits any outward dimensional growth. No visual signs of softening, distortion, or surface blistering were observed in macroscopic inspection or in SEM micrograp of the ring cross-section after 1000 h (Fig. 10a).

3.4. Lubricant oxidation and TAN evolution

The total acid number (TAN) of lubricant from the brass ring tests increased progressively with operating hours, reaching values consistent with established condemnation thresholds by 500–1000 h, driven by the catalytic effect of dissolved Cu and Zn ions on hydrocarbon oxidation chain reactions. In contrast, TAN in lubricant from the E1 composite ring tests remained at or near the baseline value of fresh ISO VG 68 oil throughout the 1000 h test duration, confirming that elimination of metallic debris directly suppresses lubricant oxidative degradation.[65–70] The mechanistic framework governing acid transport through the epoxy matrix, including a three-stage diffusion model and its temperature dependence across operational envelopes beyond the tested 55 °C condition, is developed in Section S9.

3.4.1. Long-term composite stability and nonmetallic particulate release. Beyond the absence of measurable metallic contamination, a complete assessment of lubricant cleanliness requires consideration of whether the composite ring itself releases nonmetallic particulates, specifically, epoxy matrix fragments and E-glass fibre splinters, into the oil during long-term operation. Three categories of nonmetallic debris are physically possible from the E1 ring system: (i) epoxy matrix flakes, produced by adhesive and fatigue wear at the ring–shaft contact zone and liberated as low-density, irregularly shaped fragments with Vickers hardness of ∼15–25 HV; (ii) E-glass fibre end-fragments, produced by fibre pull-out at individual asperity contacts and potentially angularly shaped with hardness ∼500–600 HV; and (iii) nanoscale silane sizing residue, detached from fibre surfaces at sub-LOQ concentrations during interfacial micro-sliding events. The gravimetric wear data provide a direct upper-bound estimate of the total nonmetallic debris dose: the composite ring lost 0.73 mg over 1000 h into a 2.5 L oil sump, corresponding to a maximum theoretical debris concentration of 0.29 ppm by mass, assuming conservatively that the entire wear mass exists as discrete suspended particles rather than surface transfer films. This concentration is three to four orders of magnitude below the metallic contamination levels measured in the brass ring oil samples (Cu: 412 ppm, Zn: 387 ppm at 1000 h) (Fig. 11d), and is negligible relative to any established particulate cleanliness threshold for rolling element bearing lubrication systems. At this concentration, even if all composite debris particles were at the coarsest end of the wear-generated size spectrum (∼100 μm glass fibre fragments), the total particle number in the oil sump would be insufficient to populate a measurable count in an ISO 4406 particle counter, an inference that is consistent with the stable bearing housing temperature and oil flow rate recorded throughout the 1000 h test, both of which are sensitive indicators of progressive lubricant contamination (Fig. 11a and b).

3.4.2. Filtration compatibility and lubricant cleanliness classification. The practical significance of nonmetallic composite debris must be evaluated not only in terms of particle hardness and concentration but also in terms of its compatibility with standard industrial lubricant filtration systems, a dimension that decisively distinguishes composite ring debris from the metallic contamination generated by the brass ring. Standard fibreglass-medium pressure filters used in industrial circulating lubrication systems, rated at $\beta_{10} \geq 75$ per ISO 16889, are specifically designed to capture particles in the ≥10 μm size range at single-pass collection efficiencies exceeding 75%. E-glass fibre fragments and epoxy matrix flakes of this size, which constitute the dominant particle type from composite ring wear, are therefore efficiently removed from the oil stream in a single filtration pass, preventing their recirculation through the rolling element bearing contact zone. Epoxy matrix flakes, being soft (HV ∼ 15–25) and deformable, will also tend to smear and embed in the filter media rather than pass through, further reducing their effective concentration in the filtered oil. Critically, the dissolved Cu^{2+} and Zn^{2+} ions released by the brass ring, detected at 412 ppm and 387 ppm respectively after 1000 h, are ionic species in solution and are entirely unaffected by mechanical filtration at any commercially practical pore size rating. These dissolved metallic contaminants remain permanently active in the oil as catalysts for oxidation chain reactions and acid generation, driving TAN to 1.035 mg KOH per g at 500 h regardless of the filtration system employed. The composite ring system thus provides a qualitatively superior contamination profile: the small quantity of nonmetallic particulate it generates is filterable by existing standard infrastructure, whereas the metallic contamination from brass rings represents a chemically irreversible degradation pathway that no filtration system can address.

The internationally accepted framework for quantifying total lubricant particulate cleanliness is ISO 4406: 2021, which assigns a three-number cleanliness code based on particle counts per millilitre at size thresholds of ≥4 μm(c), ≥6 μm(c), and ≥14 μm(c), measured by an automatic particle counter (APC) calibrated per ISO 11171. This method detects all particles regardless of composition, metallic, ceramic, polymeric, or fibrous, and therefore provides a single metric that captures the aggregate contamination burden from both ring material systems on a directly comparable basis. Typical cleanliness targets for general industrial bearing applications are ISO 16/14/11, whereas precision bearing systems, such as the SKF 6207-2Z deep-groove ball bearings in the present test rig, warrant a target of ISO 15/13/10 or cleaner. The brass ring system, generating Cu at 412 ppm and Zn at 387 ppm in association with extensive oxidation products (TAN = 1.035 mg KOH per g), almost certainly produced a cleanliness code well in excess of ISO 20/18/15 based on equivalent metallic particulate contamination data in the literature. The composite ring system, with total debris generation of ≤0.29 ppm and TAN remaining at 0.24 mg KOH per g after 1000 h, is expected to maintain an oil cleanliness code approaching that of fresh, uncontaminated ISO VG 68 mineral oil (typically ISO 14/12/9). It must be acknowledged, however, that automatic particle counting per ISO 4406 was not performed in the present study, and a formal cleanliness code cannot therefore be assigned to either oil sample set. This constitutes a defined analytical limitation: the

claim of superior lubricant cleanliness for the composite ring system is strongly supported by the AAS metallic element data, TAN results, and gravimetric wear mass differential, but would be definitively confirmed by ISO 4406 particle counting, which is recommended as a high-priority addition to any follow-on investigation.

The present study characterised lubricant contamination using atomic absorption spectrometry (GFAAS) for dissolved Cu, Zn, and Fe, and by potentiometric titration for TAN, methods that fully capture ionic metallic contamination and oil oxidation state but are analytically blind to non-metallic suspended particulates. A complete characterisation of total lubricant cleanliness per ISO 4406: 2021 would require automatic particle counting (APC) calibrated to ISO 11171, which detects all particles regardless of composition at size thresholds of $\geq$4 μm(c), $\geq$6 μm(c), and $\geq$14 μm(c) and enables assignment of a formal three-number ISO cleanliness code. Complementary analytical ferrography per ISO 4407 and direct optical microscopy would enable morphological classification of any composite wear debris, distinguishing epoxy matrix flakes from glass fibre fragments on the basis of refractive index and aspect ratio under polarised light, and would provide the most direct experimental answer to questions about the nature and size distribution of nonmetallic particles released by the composite ring. These characterisation methods are strongly recommended for any follow-on study, and their absence represents the primary analytical boundary of the current lubricant cleanliness dataset. Additionally, the abrasivity of glass fibre fragments under recirculating lubrication conditions warrants targeted future investigation using a pin-on-disc tribometer in which pre-sized glass fibre particles (10–100 μm) are introduced as a third-body abrasive in ISO VG 68 mineral oil at concentrations representative of the gravimetric estimate ($<$0.3 ppm), enabling direct quantification of their specific wear effect on bearing steel surfaces.

3.5. Nature and tribological consequences of composite wear debris

Although the epoxy–glass composite ring eliminates metallic contamination entirely, it is necessary to consider the nature and tribological consequences of the nonmetallic wear debris it generates, specifically, epoxy matrix fragments and E-glass fibre end-splinters released at the ring–shaft contact interface. The abrasive potential of any wear particle is governed primarily by its hardness relative to the bearing raceway surface and its concentration in the lubricant. Table 5 presents a comparative assessment of the relevant hardness values and primary damage modes for the three principal particle types present in this lubrication system.

Epoxy matrix debris ($\sim$15–25 HV) is substantially softer than both the brass wear particles ($\sim$100–150 HV) it replaces and the bearing steel raceways ($\sim$850–900 HV), placing it firmly below the abrasivity threshold at which hard-body ploughing of raceway surfaces occurs. It is therefore tribologically benign and is more likely to form thin, compliant transfer films at contact surfaces than to generate abrasive micro-cutting damage. E-glass fibre fragments are harder ($\sim$500–600 HV, approximately 60% of bearing steel hardness) and more angularly shaped than brass particles, and therefore carry a higher per-particle abrasive potential if they recirculate through the rolling contact zone. However, the key mitigating factor is the total debris dose: the composite ring generated a gravimetric wear mass of only 0.73 mg over 1000 h of operation, compared with 1847 mg for the brass ring, a differential of more than 2500-fold [Table 2]. At the measured wear rate, the theoretical maximum debris concentration from the composite ring in the 2.5 L oil sump is less than 0.3 ppm by mass, three to four orders of magnitude below the metallic contamination levels measured in the brass ring tests (Cu: 412 ppm, Zn: 387 ppm at 1000 h). Since bearing surface damage is governed by the combined product of particle hardness, concentration, and size, not hardness alone, this extreme difference in total debris dose is the decisive factor establishing that the composite ring system poses a negligible abrasive risk to bearing precision under the tested conditions. Furthermore, glass fibre fragments, owing to their high aspect ratio, preferentially align parallel to flow streamlines in the oil sump and are efficiently captured by standard fibreglass-medium filter elements rated at $\beta_{10} \geq 75$ (ISO 16889) in a single pass through the lubrication circuit, a self-limiting contamination behaviour well documented for fibre-reinforced polymer tribopairs. By contrast, the dissolved Cu^{2+} and Zn^{2+} ions generated by the brass ring are not removable by mechanical filtration and remain permanently active as catalysts for lubricant oxidation throughout the oil service life.

From a tribological standpoint, the relative abrasivity of particles is governed by their hardness relative to the bearing raceway material (typically bearing steel, $\sim$700 HV). Metallic Cu and Zn particles released from a brass ring possess Vickers hardness values in the range of 100–180 HV, yet in finely divided form they can act as three-body abrasives that generate grooves on softer counterfaces and accelerate oxidative wear. Glass fibres (E-glass, Vickers hardness $\approx$ 550–600 HV) are inherently harder than copper or zinc and could, in principle, be more abrasive if released in large quantities with sharp morphologies. However, the quantitative SEM evidence presented in Table 4

Table 5 Hardness and damage characteristics of wear particles relevant to the present system

Particle type	Mohs hardness	Vickers hardness (HV)	Primary damage mode	Filterable by $\beta_{10} \geq 75$?
Epoxy matrix flakes	$\sim$2–3	$\sim$15–25	Film formation, embedding	Yes
E-glass fibre fragments	$\sim$5.5–6	$\sim$500–600	Micro-cutting, ploughing	Yes ($>$10 μm)
CuZn30 brass particles	$\sim$3–4	$\sim$100–150	Surface fatigue, denting	Yes
Bearing steel (SAE 52100)	$\sim$8.5	$\sim$850–900	Reference surface	—

(fibre pull-out density < 0.3 fibres mm^{-2}; crack density < 0.02 mm mm^{-2}; ΔR_a < 0.05 μm after 1000 h) confirms that fibre release under the present operating conditions is minimal and below levels reported to cause measurable bearing damage in comparable polymer composite tribological studies [ref. 66–68]. By contrast, the copper alloy ring released Cu and Zn at 241 and 568 ppm, respectively, concentrations orders of magnitude higher than any incidental non-metallic debris, causing measurable shaft wear and elevated TAN. Future tests incorporating optical particle counters and ISO 4406 cleanliness classification should be performed to establish firm cleanliness limits for the composite ring system.

3.6. Fibre–matrix interfacial integrity

Post-test SEM examination confirmed that the fibre–matrix interface in the E1 ring remained structurally intact after 1000 h of operation in ISO VG 68 oil at 55 °C, with no evidence of silane bond hydrolysis, interfacial delamination, or acid-driven debonding under the tested conditions.[71,72] This observation is consistent with the low TAN values maintained in the E1 lubricant, which precluded the acidic interfacial attack that would be expected at TAN levels approaching or exceeding the condemnation limit.[73,74] The molecular dynamics framework for interfacial debonding kinetics and the predicted debonding onset conditions at elevated acid concentrations and temperatures are provided in Section S10 for reference in future studies extending the operational envelope.

3.7. Economic evaluation

A three-level cost analysis, spanning raw material unit cost, manufacturing cost at scale, and operational life-cycle economics, consistently favours the epoxy–glass composite ring over conventional brass. At the material level, the composite ring offers a 7–10× reduction in raw material cost per unit, driven by the low cost of epoxy resin and E-glass relative to LME-priced copper alloy feedstock. At the manufacturing level, near-*net*-shape casting of the composite ring eliminates the CNC turning operations required for brass rings, further reducing per-unit production cost at moderate-to-high volumes, notwithstanding a non-trivial multi-cavity mould tooling investment that must be amortised over sufficient production runs. At the operational level, the composite ring extends lubricant service life by approximately 2×, by eliminating metal-catalysed oil oxidation, and projects a ring replacement interval 3–5× longer than that of brass rings based on the measured gravimetric wear rate of 7.3×10^{-4} mg h^{-1}; each avoided replacement event eliminates a system shutdown, bearing housing disassembly, and recommissioning cycle. The composite ring's economic advantage is therefore most clearly realised at moderate-to-high production volumes and over operational horizons of two years or more, conditions routinely met in continuous industrial rotating machinery. Full pricing assumptions, cost derivations, maintenance frequency calculations, and life-cycle cost projections are provided in the Supplementary Economic Impact Supplement (SI Section S8).

From an industrial implementation perspective, the present epoxy–glass ring combines a simple near-*net*-shape fabrication route already demonstrated by open-mould casting, a favourable projected cost profile relative to CNC-machined brass, and a clearly defined thermal operating window based on the measured matrix T_g of 110 °C and the observed service maximum of 55 °C, while applications above about 80–90 °C should be validated separately or transitioned to higher-T_g matrix systems.

3.8. Placement within the current state of knowledge

Polymer and composite materials are increasingly adopted in bearing and sealing applications because they offer lower density, corrosion resistance and favourable tribological behaviour compared with traditional metallic alloys. Recent studies on polymer-based bearing and seal materials—such as TPU- and PTFE-based composites or polymer overlays on engine bearings—report substantial reductions in friction and wear, particularly under mixed or boundary lubrication, mainly due to their ability to form protective transfer films and to avoid adhesive metal–metal contact. However, these investigations typically focus on sliding or journal bearings and do not address splash-ring components where lubricant transport, metallic debris generation and lubricant degradation are tightly coupled.[75–77]

The present results extend this body of knowledge by demonstrating that replacing a conventional brass oil splash ring with a lightweight epoxy–glass composite not only reduces wear of the ring itself but also virtually eliminates metallic contamination of the lubricant (Cu, Zn, Fe below quantification limits) and the associated increase in TAN over 500–1000 h of service. In contrast, studies on metallic bronze or brass-bearing materials often report substantial metal pick-up in the lubricant and a strong link between metallic debris, accelerated oxidation, and lubricant failure, consistent with the high Cu and Zn concentrations and elevated TAN observed here for the copper alloy ring. The composite ring, therefore, breaks the well-known failure chain "metal wear → debris contamination → lubricant oxidation → further wear" that has been described in both industrial case studies and controlled tribology experiments on metal-based systems.[78,79]

From a lubrication-mechanism perspective, previous work on polymer-faced or polymer-coated bearings has shown that compliant polymer layers can support hydrodynamic film formation while reducing breakaway friction and vibration, particularly in start–stop or low-speed conditions. The present study shows a similar benefit in a splash-lubricated configuration: the reduced inertia and smoother, more stable motion of the composite ring increase oil delivery by about 66% and reduce bearing temperatures by roughly 3 °C compared with the metallic ring, without inducing additional wear or debris formation. In this way, the work complements existing research on polymer bearings by demonstrating that a carefully designed epoxy–glass composite ring can simultaneously act as a low-wear structural component and as an efficient oil distributor that preserves lubricant integrity, a combination that has not been explicitly reported for oil splash rings in the available literature.[80,81]

Despite the positive tribological and lubricant-quality results reported here, several limitations should be acknowledged.

First, the tests were conducted under a single shaft speed, load configuration, and lubricant type, so the performance of the composite ring in other operating envelopes (*e.g.*, higher temperatures, different viscosities, contaminated or degraded oils) remains to be quantified. Second, the epoxy–glass composite has a finite maximum operating temperature and may be more sensitive to thermal ageing and chemical attack than high-temperature metallic alloys, which could restrict its use in very high-temperature environments. Third, manufacturing costs, process variability, and quality control for large-scale composite ring production have not been evaluated in this study and will affect the practical cost–benefit balance relative to conventional metallic rings. Future work should address these aspects through extended service tests, environmental ageing studies and a techno-economic assessment of composite ring manufacturing and deployment.

4. Conclusion

This study has convincingly established that an oil splash ring made of a 90 : 10 wt% epoxy-glass fibre composite is an excellent alternative to conventional metallic rings for the performance of bearing lubrication in high-speed rotating machines. Agreements otherwise are an extension of the proposition that recoil rings possess operational properties equal to, or indeed superior to, those of metals, resisting modes of failure in almost all push tests.

The following is a summary of the results obtained:

• The composite splash ring reduced metallic wear-debris contamination of the lubricant to below the AAS detection limit (Cu, Zn and Fe all <0.1 ppm under the present test conditions), effectively eliminating measurable metallic debris in this study. However, the possibility of non-metallic debris from the epoxy matrix or glass fibres is not addressed by the present elemental analysis and should be investigated in future work.

• Improved lubrication and thermal performance: the oil delivery was increased by 66% due to reduced weight and increased dynamic stability of the composite ring, resulting in more efficient bearing lubrication and a lower stable operating temperature.

• Proof of longevity and strength: this collective evidence of material durability extended beyond 1000 h of testing, finite element analysis, and scanning electron microscopy. The ring has a strong structural design, which will be highly resistant to various wear and fatigue mechanisms affecting other materials used in this particular application.

This contribution extends further than just material substitution. It successfully provides a validated, readily implementable engineering solution to a long-established and critical reliability issue right at its source. The epoxy-glass fibre composite ring will eliminate the cascade of failure modes from wear, through contamination, into lubricant degradation, by providing for a multitude of significant improvements in operational reliability and extension of service life for bearings in many industrial applications, from pumps and compressors to all other rotating machinery.

Continuing research should focus on examining the performance of this composite ring under even harsher operating conditions, such as higher speeds, loads, and temperatures, to provide a more complete picture of the performance spectrum of the composite. For future research, equally important are investigations at elevated temperatures (80 °C and up to 120 °C), where properties of the epoxy matrix may undergo thermal degradation, and at sub-zero temperatures (down to −40 °C) to simulate cold-start conditions. Long immersion studies in hot synthetic oils can also be performed to check for degradation of the material and swelling, while a sensible subsequent step would be to look into a second-generation self-lubricating composite by introducing suitable solid lubricants like PTFE or graphite into the epoxy-glass matrix, which is one of the most commonly used techniques to enhance the tribological performance of polymer bearings.

Building on the present findings, future investigations should systematically examine composite ring performance across a matrix of lubricant temperature and acid value conditions to establish the full operational envelope of the E1 epoxy–glass system. A minimum recommended test matrix comprises: oil temperatures of 25 °C (present baseline), 80 °C, and 120 °C, each combined with initial TAN values of 0.15 mg KOH per g (fresh oil, present baseline), 1.0 mg KOH per g (moderately aged, approaching industrial condemnation limit), and 2.0 mg KOH per g (severely degraded, simulating end-of-service conditions). For each condition, the key performance indicators should include gravimetric mass uptake per ASTM D570, dimensional stability (outer diameter, ring width, and shaft clearance), flexural modulus retention per ASTM D790 on aged coupon specimens immersed under the same conditions, and SEM characterisation of fibre–matrix interfacial integrity after exposure. At temperatures approaching 120 °C, which represents approximately 55% of the measured T_g (110 °C) of the Araldite LY 1564/Aradur 3486 matrix, DMA should be used to quantify any plasticisation-induced reduction in storage modulus, as this would provide direct evidence of the onset of matrix softening under realistic service conditions. If elevated-temperature performance is found to be limiting, a straightforward material upgrade pathway exists: substitution of the polyamide-cured matrix with an anhydride-cured or novolac-cured epoxy system ($T_g \sim$ = 150–200 °C) would extend the thermal operating envelope without changing the ring geometry or fabrication route, preserving theear-*net*-shape manufacturing and cost advantages demonstrated in the present study. Equally important for future work is the introduction of solid lubricant additives, such as PTFE particles or graphite flakes, into the epoxy–glass matrix, which are well-established strategies for reducing the friction coefficient of polymer composites under boundary lubrication conditions and would further improve tribological performance during transient operating phases.

Conflicts of interest

There are no conflicts to declare.

Data availability

The datasets generated and analysed during the current study are available in this article. Raw experimental data, including oil analysis measurements, tribological test results, and microscopy images, are available from the corresponding author upon reasonable request. Supplementary information (SI) is available. See DOI: https://doi.org/10.1039/d6ma00365f.

References

1 D. R. H. Jones and M. F. Ashby, Case Studies in Friction and Wear, *Engineering Materials 1: An Introduction to Properties, Applications and Design*, Elsevier Ltd, 5th ed., 2019, pp. 485–497, DOI: 10.1016/C2015-0-04446-X.
2 Q. Peng, L. Gui and Z. Fan, *Engineering Applications of Computational Fluid Mechanics*, 2018, **12**, 324–333.
3 A. Lycksam, M. O'Nils and F. Z. Qureshi, *IEEE Access*, 2025, **13**, 91682–91692.
4 L. Wang, D. Ping, C. Wang, S. Jiang, J. Shen and J. Zhang, *Processes*, 2023, **11**, 1928.
5 I. Wilińska and S. Wilkanowicz, *Energies*, 2025, **18**, 4006.
6 X. Deng, S. Wang, Y. Hammi, L. Qian and Y. Liu, *Tribol. Int.*, 2020, **146**, 106261.
7 U. Koklu and S. Morkavuk, *Surf. Rev. Lett.*, 2019, **26**, 1950060.
8 L. Wang, L. Hu, J. Zhang and J. Liao, *Proc. Inst. Mech. Eng., Part C*, 2025, **239**(5), 1607–1623.
9 H. P. Bloch and A. R. Budris, *Pump User's Handbook*, River Publishers, 2021.
10 B. P. Aramide, A. P. I. Popoola, E. R. Sadiku, F. O. Aramide, T. Jamiru and S. L. Pityana, in *Handbook of Nanomaterials and Nanocomposites for Energy and Environmental Applications*, Springer International Publishing, Cham, 2021, pp. 731–755.
11 U. Köklü, O. Demir, A. Avcı and A. Etyemez, *J. Mech. Sci. Technol.*, 2017, **31**, 4703–4709.
12 M. M. Nemat-Alla, A. M. Gad, A. A. Khalil and A. M. Nasr, *J. Tribol.*, 2009, **131**(1), 011701.
13 Z. Eusufzai, *ASRC Proc.*, 2025, **01**, 618–653.
14 P. Choi and A. Rudin, in *The Elements of Polymer Science and Engineering*, Elsevier, 2026, pp. 1–36.
15 P. K. Mallick, *Fiber-Reinforced Composites*, CRC Press, 2007.
16 P. Morampudi, K. K. Namala, Y. K. Gajjela, M. Barath and G. Prudhvi, *Mater. Today Proc.*, 2021, **43**, 314–319.
17 S. Morkavuk, U. Köklü, M. Bağcı and L. Gemi, *Compos. B Eng.*, 2018, **147**, 1–11.
18 Y. Wen, C. Chen, Y. Ye, Z. Xue, H. Liu, X. Zhou, Y. Zhang, D. Li, X. Xie and Y. Mai, *Adv. Mater.*, 2022, **34**(52), 2201023.
19 K. Friedrich, *Adv. Ind. Eng. Polym. Res.*, 2018, **1**, 3–39.
20 M. M. A. Baig and M. A. Samad, *Polymers*, 2021, **13**, 179.
21 J. J. Fekiač, M. Krbata, M. Kohutiar, R. Janík, L. Kakošová, A. Breznická, M. Eckert and P. Mikuš, *Polymers*, 2025, **17**, 271.
22 S. Kumar and K. Singh, *Proc. Inst. Mech. Eng., Part L*, 2020, **234**, 1439–1449.
23 E. Omrani, P. L. Menezes and P. K. Rohatgi, *Eng. Sci. Technol.*, 2016, **19**, 717–736.
24 C. Birleanu, M. Cioaza, F. Serdean, M. Pustan, P. Bere and G. Contiu, *Polymers*, 2023, **16**, 62.
25 G. Xian, X. Qi, R. Guo, J. Tian, H. Xiao and C. Li, *Polymers*, 2024, **16**, 3446.
26 Z. Zhang, G. Hou, H. Wan, J. Ma, T. Wang, F. Dong, L. Chen, Y. An, H. Zhou and J. Chen, *Chem. Eng. J.*, 2025, **526**, 171066.
27 A. Patnaik, A. Satapathy, S. S. Mahapatra and R. R. Dash, *J. Reinf. Plast. Compos.*, 2009, **28**, 513–536.
28 L. Lei, M. Tang, Y. Huang, Y. Zhou, J. Zheng, L. Song, E. Zhang and Z. Zhou, *Tribol. Int.*, 2025, **212**, 110954.
29 W. Huang, G. Feng, H. He, J. Chen, J. Wang and Z. Zhao, *Pet. Sci.*, 2022, **19**(3), 1305–1321.
30 A. Dinită, R. G. Ripeanu, C. N. Ilincă, D. Cursaru, D. Matei, R. I. Naim, M. Tănase and A. I. Portoacă, *Polymers*, 2024, **16**(1/2), 16010002.
31 A. K. Hamzat, F. Altun, F. Yeasmin, N. Unlu, E. Bahceci, E. Asmatulu, M. Bakir and R. Asmatulu, *Polym. Degrad. Stab.*, 2025, **242**, 111679.
32 S. V. Panin, V. O. Alexenko and D. G. Buslovich, *Polymers*, 2022, **14**, 975.
33 N. Singh and S. K. Sinha, *Proc. Inst. Mech. Eng., Part J*, 2025, **239**, 363–374.
34 M. Yin, X. Chen, Y. Dai, D. Yang, L. Xu and X. Zhu, *Aerospace*, 2021, **8**, 345.
35 D. Abraham, S. Matthews and R. McIlhagger, *Compos. Part A Appl. Sci. Manuf.*, 1998, **29**, 795–801.
36 L. Laiarinandrasana, C. Devilliers, S. Oberti, E. Gaudichet, B. Fayolle and J. M. Lucatelli, *Int. J. Pressure Vessels Piping*, 2011, **88**, 1–10.
37 A. Neurouth, C. Changenet, F. Ville, M. Octrue and E. Tinguy, *J. Tribol.*, 2017, **139**(6), 061104.
38 U. Koch and U. Wallner, *MTZ worldwide*, 2021, **82**, 48–53.
39 B. Jakubek, K. Grochalski, W. Rukat and H. Sokol, *Measurement*, 2022, **189**, 110512.
40 *GT STRUDL: The Unsung Superhero of Structural Analysis*, https://aliresources.hexagon.com/cadworx-analysis-solutions/gt-strudl-the-unsung-superhero-of-structural-analysis, (accessed 12 August 2025).
41 C. L. Tucker III and E. Liang, *Compos. Sci. Technol.*, 1999, **59**, 655–671.
42 J. C. H. Affdl and J. L. Kardos, *Polym. Eng. Sci.*, 1976, **16**, 344–352.
43 S. Fu, *Compos. Sci. Technol.*, 1996, **56**, 1179–1190.
44 E. J. Barbero, *Finite Element Analysis of Composite Materials Using Ansys®*, CRC Press, 2013.
45 J. Holmgren, J. Heinrichs Lindgren, Å. Kassman Rudolphi and S. Jacobson, *J. Appl. Polym. Sci.*, 2024, **141**(9), e55027.
46 J. M. Khare, S. Dahiya, B. Gangil, L. Ranakoti, S. Sharma, M. R. M. Huzaifah, R. A. Ilyas, S. P. Dwivedi, S. Chattopadhyaya, H. C. Kilinc and C. Li, *Polymers*, 2021, **13**, 3607.
47 M. İ. Özsoy, M. Ö. Bora, S. Ürgün, S. Fidan and E. Güleç, *Polymers*, 2025, **17**, 2944.
48 I. Sabry, A.-H. I. Mourad, A. Subhan and A. H. Idrisi, *2022 Advances in Science and Engineering Technology International Conferences (ASET), IEEE*, 2022, pp. 1–4.

49 H. Xia, J. Li, K. Wang, X. Hou, T. Yang, J. Hu and Z. Shi, *Adv. Compos. Hybrid Mater.*, 2022, **5**, 173–183.
50 D. Xia, Y. Wang, H. Liu, J. Yan, H. Lin and S. Han, *Lubricants*, 2024, **12**, 115.
51 O. Lacroix-Andrivet, M. Hubert-Roux, C. Loutelier Bourhis, S. Moualdi, A. L. Mendes Siqueira and C. Afonso, *Lubricants*, 2023, **11**, 345.
52 J. Fitch and B. Fitch, in *Condition Monitoring, Troubleshooting and Reliability in Rotating Machinery*, Wiley, 2023, pp. 87–134.
53 P. A. P. Decote, L. Negris, A. P. Vidoto, L. A. N. Mendes, E. M. M. Flores, M. A. Vicente and M. F. P. Santos, *Fuel*, 2022, **313**, 122642.
54 F. Zhou, J. Shen, X. Li, K. Yang and L. Wang, *Lubricants*, 2025, **13**, 355.
55 W. Chokelarb, P. Sriprom, L. Permana and P. Assawasaengrat, *Heliyon*, 2024, **10**(18), e37486.
56 Y. Xu, Z. Guo, X. Rao, H. Yin, S. Jiang, M. Wu, L. Zhou and C. Yuan, *Lubrication Sci.*, 2025, **37**, 283–302.
57 P. Pitakjakpipop, T. Khudkham, W. Anutrasakda, N. Kornkanlaya, H. Pitakjakpipop, N. Khamtep, P. Watcharapo and N. Phiromphu, *Fuel*, 2026, **407**, 137253.
58 D. A. Duque-Sarmiento and D. A. Baño-Morales, *Lubricants*, 2024, **12**, 320.
59 B. Aldousiri, A. Shalwan and C. W. Chin, *Adv. Mater. Sci. Eng.*, 2013, **2013**, 1–8.
60 M. G. Jacko, P. H. S. Tsang and S. K. Rhee, *Wear*, 1989, **133**, 23–38.
61 N. Kumar, G. Setia, T. Nanda, V. Singh, R. Mehta and A. Bansal, *Wear*, 2026, **584–585**, 206389.
62 A. Chasalevris, *Int. J. Rotating Mach.*, 2016, **2016**, 1–22.
63 P. W. R. Beaumont, *Appl. Compos. Mater.*, 2020, **27**, 449–478.
64 H. Guo, S. Du, J. Lei, Y. Zhang and L. Hu, *Front. Mater.*, 2019, **6**, 00162.
65 M. H. Moosa, M. Abu-Okail, A. Abu-Oqail, S. A. Al-Shelkamy, W. M. Shewakh and M. A. Ghafaar, *Polymers*, 2023, **15**, 2064.
66 S. Fidan, S. Ürgün, M. İ. Özsoy, M. Ö. Bora and E. Güleç, *Polymers*, 2025, **17**, 2503.
67 Y. Meng, J. Xu, L. Ma, Z. Jin, B. Prakash, T. Ma and W. Wang, *Friction*, 2022, **10**, 1443–1595.
68 C. A. Chairman, M. Ravichandran, V. Mohanavel, T. Sathish, A. Rashedi, I. M. Alarifi, I. A. Badruddin, A. E. Anqi and A. Afzal, *Materials*, 2021, **14**, 5257.
69 M. Korku, R. İlhan and E. Feyzullahoğlu, *Polym. Compos.*, 2025, **46**, 355–371.
70 S. Shan Zhou, J. Jian Song, P. Xu, M. He, M. Biao Xu and F. Chang You, *Geoenergy Sci. Eng.*, 2023, **229**, 212074.
71 D. Liao, T. Gu, J. Liu, S. Chen, F. Zhao, S. Len, J. Dou, X. Qian and J. Wang, *Compos. B Eng.*, 2024, **270**, 111131.
72 X. Q. Wang, W. Jian, O. Buyukozturk, C. K. Y. Leung and D. Lau, *Compos. B Eng.*, 2021, **206**, 108534.
73 X. Liu, B. Wang, Q. Su, Q. Zuo and X. Song, *Polymers*, 2023, **15**, 2278.
74 M. Rojek, J. Stabik and S. Sokół, *J. Achiev. Mater. Manuf. Eng.*, 2007, **20**, 183–186.
75 M. Chernets, R. Wrona and Y. Chernets, *Sci. J. Sil. Univ. Technol., Ser. Transp.*, 2024, **123**, 5–21.
76 I. Ozdemir, B. Bulbul, U. Kiracbedel, T. Grund and T. Lampke, *Materials*, 2024, **17**, 3802.
77 S. Jiang, J. S. S. Wong, D. Puhan, T. Yuan, X. Bai and C. Yuan, *Friction*, 2024, **12**, 1801–1815.
78 G. Jacobs and M. Plogmann, in *Encyclopedia of Lubricants and Lubrication*, Springer Berlin Heidelberg, Berlin, Heidelberg, 2014, pp. 1618–1633.
79 L. Zhao, J. Li, Q. Yang, Y. Wang, X. Zhang, H. Li, Z. Yang, D. Xu and J. Liu, *Crystals*, 2022, **12**, 834.
80 M. Santeramo, G. Giannetti, E. Meli, G. Carbone and C. Putignano, *Tribol. Int.*, 2026, **213**, 111010.
81 E. A. Bolgova, M. A. Mukutadze and V. M. Prihod'ko, *Vestnik IzhGTU imeni M.T. Kalashnikova*, 2024, **27**, 14–21.